nature portfolio

Peer Review File

SARS-CoV-2 NSP14 inhibitor exhibits potent antiviral activity and reverses NSP14-driven host modulation

Corresponding Author: Professor Wei Xie

This manuscript has been previously reviewed at another journal. This document only contains information relating to versions considered at Nature Communications.

This file contains all reviewer reports in order by version, followed by all author rebuttals in order by version.

Version 0:

Reviewer comments:

Reviewer #1

(Remarks to the Author)
Luo, et al, presented a non-nucleoside inhibitor of the SARS-CoV-2 NSP14 SAM-binding pocket, C10, which demonstrates robust antiviral activity against SARS-CoV-2, including its variants, comparable to remdesivir. And C10 could specifically reversed NSP14-mediated alterations in host transcriptome and restored host cell cycle progression disrupted by NSP14. This work pointed out the C10 as a promising candidate for the development of effective treatments against SARS-CoV-2 and its emerging variants and also uncovers a novel mechanism of NSP14 in SARS-CoV-2 pathogenesis and its therapeutic potential. It is a topic of interest to the researchers in the related areas but the paper needs very some improvement before acceptance for publication. My detailed comments are as follows:

1.This work proposed that C10 can specifically bind in the SAM pocket of nsp14 and affect the capping process, thus inhibiting viral proliferation, but there are not enough biochemical experiments to prove that C10 inhibits the MTase of nsp14, and supplemental thin-layer chromatography analysis is recommended .
Reference: Y. Chen, H. Cai, J. Pan, N. Xiang, P. Tien, T. Ahola, & D. Guo, Functional screen reveals SARS coronavirus nonstructural protein nsp14 as a novel cap N7 methyltransferase, Proc. Natl. Acad. Sci. U.S.A. 106 (9) 3484-3489, https://doi.org/10.1073/pnas.0808790106 (2009).
2.Line 134-135: “The key residues for the binding of C10 to NSP14 predicted by the MM/GBSA free energy decomposition are listed in Fig. 2b.”
I think there is a clerical error. The key residues are listed in Fig. 3b.
3.Line 135-138: “The predicted structure of SARS-CoV-2 NSP14 bound to C10 and GpppG in a space-filling representation is shown in Fig. 3c. An expanded view of the bound C10 and GpppG (Fig. 3d) characterized a narrow binding pocket for C10, adjacent to the RNA cap-binding site.”
7BIF is a crystal structure of SARS-CoV-2 NSP14 in complex with 7MeGpppG instead of GpppG, and is similarly mislabeled in Fig. 3c, 3d and 3e.
4.Line 141-143: “First, the stronger electronegativity of the phenyl trifluoromethyl group in C10 provides additional electrostatic interactions with a druggable site (refers to site-C) composed of residues Arg310, Gln313, Asp331, Cys340, and Trp385.”
It would be useful to also label the interactions between fluoromethyl groups and site-C residues with a dashed line on Fig. 3g.
5.Line 232-233: “A Venn diagram analysis showed a significant overlap of the differentially expressed genes induced by NSP14 expression and those induced by NSP14 inhibition mediated by C10 (Fig. 5f).”
In Fig. 5f, we can see the overlap of the upregulated genes induced by NSP14 expression and downregulated genes induced by C10, and vice versa. But, is there also an overlap between the upregulated genes induced by NSP14 expression and the upregulated genesafter the induced by C10, or he downregulated genes induced by NSP14 expression and the downregulated genesafter the induced by C10?

Reviewer #2

(Remarks to the Author)

The manuscript describes the identification of a novel antiviral drug targeting the SARS-CoV-2 NSP14 N7-guanine-methyltransferase activity. A robust medicinal chemistry virtual screening approach followed by lead optimization identified the compound C10 for further characterisation. Biochemical/biophysical analysis confirmed the SAM pocked as the target and virtual SAR defined the involved residues in the pocket. Infection assays confirmed antiviral activity in the low micromolar down to nanomolar for the Omicron variants, with a good SI. The compound is specific for Coronavirus MTase and more potent for SARS-CoV-2 than NCoV-OC43. They then show that C10 inhibits viral replication and reversed NSP14 modulation of the host transcriptome and NSP14 induced cell cycle arrest. Finally, they tested antiviral efficacy in vivo in the K18-hACE2 transgenic mouse model for SARS-CoV-2 infection.
The importance of identifying novel targets for antiviral therapy of SARS-CoV-2, and viruses in general, is highlighted also by the recent work by Mayer et al (Nature 2025) demonstrating significant therapeutic potential of another inhibitor of NSP14 (TDI-015051) targeting the cap-binding site. Having two drugs effective for the same target with two different mechanisms might allow combination for next generation NSP14 inhibitors.
While the medicinal chemistry approach appears robust, with extensive biochemical/biophysical characterisation, the biological/virological characterisation remains incomplete, below some specific considerations:
- Data on virus inhibition start on Figure 4 with the analysis of different SARs-CoV-2 variants (lacks definition of strains, “original” is not sufficient). The experimental setup involves 1h pre-treatment with the drug prior to infection and readout at 24h. No time-of-addition experiments are shown. Activity on replication is confirmed with a replicon assay, which could be considered a surrogate test at best (Figure 5a, please use luciferase activity rather than RdRp activity). TOA is useful to understand also if the drug can act while the virus is replicating in vesicles.
- A critical experiment would be to select for resistant mutations by incubating cycles of virus infection with increasing concentrations of drug. This allows the identification of mutations in the target site of the drug and measurement of fitness of resulting viruses, all essential information for characterisation of a novel drug.
- The direct outcome of inhibition of vRNA capping would be translation defects and generation of RNA that could trigger immune sensing and virus clearance. Neither of the two outcomes has been addressed.
- Instead, the authors engage in an analysis of the effect of the drug on indirect activities of NSP14 on the cell transcriptome and cell cycle. It took me some time to understand if the MTase activity of NSP14 was required and maybe it could be useful if the authors mention this in the text and the associated reference (Zaffagni et al. eLife 2022). Discussion could include also the role of IMPDH2 as NSP14 associated protein also required for the global effect on gene expression.
- In vivo experimentation is welcome. However, more discussion of the results is needed. For example, Figure 6f shows non-significant reduction of virus titre in lungs at non-toxic concentrations (<100 mg/kg) indicating more work to optimise this class of inhibitors in vivo to reduce toxicity and increase efficacy. Figure 6j shows similar decrease of N antigen staining compared to Remdesivir control but at higher concentrations (12 mg/kg).
To conclude, although the results are promising, still the drug would require further optimisation for successful in vivo administration. Furthermore, a more accurate virological analysis would be helpful also for optimisation (i.e. binding site mutations).

Reviewer #3

(Remarks to the Author)
The circulation of SARS-CoV-2 in the human population, the occurrence of chronic infections in immunocompromised individuals or in some patients with long COVID, and the emergence of variants resistant to the limited antiviral treatments currently available all underscore the urgent need for new, effective antiviral strategies against coronaviruses. In this study, the authors identify inhibitors of the N7-methyltransferase (MTase) activity of the nsp14 protein, which is involved in synthesizing the cap structure essential for the translation of viral messenger RNAs into proteins.
Inhibition of this enzyme class using analogs of the methyl donor S-adenosylmethionine (SAM, an adenosine derivative) has already been explored by several groups, leading to the identification of selective inhibitors active, in vitro, in the nanomolar range (10–500 nM). However, most of these compounds have shown limited efficacy in infected cells.
In the present study, the inhibitors target the same catalytic pocket but are not nucleoside analogs. Using this approach, the authors identified compounds active both in vitro and in infected cells, with EC50 values ranging from 64 to 301 nM. Some antiviral efficacy was also demonstrated in a mouse model of SARS-CoV-2 infection, although the compounds appear toxic at higher doses (2,5x). Furthermore, the candidate molecules exhibit antiviral activity against multiple SARS-CoV-2 variants and prevent transcriptome remodelling observed in infected cells.
Overall, this study is well-designed and provides substantial preliminary data that may contribute to the development of new antiviral strategies against this virus family. However, while the findings are important for the field of antiviral drug development, several conclusions are not fully supported by the experimental data, and additional experiments are needed before publication in Nature Communications.

Major Comments

1. Clarification of the Mode of Action of Compound C10
The abstract, the end of the introduction, and paragraph 3 ("C10 directly inhibits the genomic replication of SARS-CoV-2") suggest a direct inhibition of viral replication by C10. However, the data presented do not support a direct effect on the viral replication machinery. Direct inhibition would imply an interaction with the viral polymerase complex, which is not demonstrated here. Instead, the compound more likely targets viral mRNA translation and modulates host transcriptome responses via an unknown mechanism. The most plausible hypothesis is that C10 interferes with viral protein synthesis, thereby limiting the production of replication complexes and in turn will modulates the replication. This hypothesis could be experimentally confirmed by analyzing C10’s effect on viral protein expression levels.

2. Figure 1 – ExoN Activity Control

It is important to demonstrate that compounds C3 and C10 do not affect the ExoN activity of nsp14, either in the presence or absence of its co-factor nsp10. This would clarify that the compounds specifically target the N7-MTase activity.

3. Figure 2 – puzzling experimental design of figure 2
Figure 2 lacks consistency. In some panels (e.g., 2B and 2H), GpppG is used, while in others (e.g., 2D), m7GpppG is tested. For robust interpretation, both analogs (GpppG and m7GpppG) as well as SAH should be tested across all relevant assays (DSF, SPR).

4. Structural Modeling and Validation of C10 Binding
The authors present a structural model of C10 bound in the SAM-binding pocket of nsp14 and offer indirect evidence of specific binding. However, crystallization of full-length nsp14 appears unsuccessful. Recent studies (PMID: 36075969, 39188530) have shown that the isolated MTase domain can be crystallized when fused with a TELSAM tag. This construct could be used to attempt co-crystallization with C10, providing direct structural confirmation.

5. Functional Analysis of Mutants
Mutational analysis indicates that Q313R and W385A are involved in C10 binding. It would be valuable to assess whether additional mutations in site-C also impact C10 binding. Moreover, it should be determined whether these mutations alter N7-MTase activity and confer resistance to C10 in a viral context. If enzymatic function is impaired, an alternative approach could be to select C10-resistant viral mutants to validate the binding model and assess the impact of these mutations on biophysical readouts (DSF, SPR). These studies would help evaluate the resistance potential of this compound class.

6. Selectivity Studies
To strengthen the manuscript, the authors should report C10's activity against MERS-CoV nsp14, given the zoonotic risk associated with this virus. Additionally, testing C10 against the human N7-MTase involved in mRNA capping is crucial to assess potential off-target effects, especially in light of the compound's in vivo toxicity at high doses (300 mg/kg in mice).

Minor Comments
1. Introduction – Functional Coupling of ExoN and MTase Domains
Please mention that although nsp14 has two distinct domains (ExoN and N7-MTase), mutagenesis studies suggest functional interdependence between them. This is important for understanding the enzyme's biology.

2. Introduction – SAM-Binding Site as a Drug Target
The sentence "However, the development of promising inhibitors targeting the NSP14 SAM-binding pocket remains underexplored" is somewhat misleading. Several groups have reported inhibitors of this pocket, including adenosine mimetics and bisubstrate analogs. While their efficacy in infected cells is limited, they demonstrate potent in vitro inhibition of N7-MTase activity. Please cite these studies for context.

3. Selectivity Studies
It would be beneficial to assess C10's activity against MERS-CoV nsp14 and human N7-MTase to evaluate cross-reactivity and to unravel the toxicity described in mouse model.
4. Results – Terminology Clarification
Please clarify the terms "standard precision" and "extra precision" modes in the context of docking analysis. Also, define MPXV at its first mention.

5. Materials and Methods – Biosafety Level
The biosafety level (BSL) used for experiments involving infectious SARS-CoV-2 should be explicitly stated.

6• Figure 3e/f – Structural Insights
The authors should discuss their findings in light of previously reported SAM entry gate in nsp14 structures (PMID 36546776).

7. Line 164 – Language Editing
The term "authentic" could be removed for clarity, unless it refers to a specific assay or strain type.

8. Cell Cycle Arrest Section
The section discussing nsp14-induced cell cycle arrest is underdeveloped mechanistically and lacks appropriate controls (e.g., catalytically inactive mutants). As it does not significantly contribute to the main conclusions, it should either be removed or moved to the supplementary information.

Version 1:

Reviewer comments:

Reviewer #1

(Remarks to the Author)
I did not have any substantial issues during the first round, and I continue to think that this paper merits publication in nature communications. It presented a non-nucleoside inhibitor of the SARS-CoV-2 NSP14 SAM-binding pocket, C10, which demonstrates robust antiviral activity against SARS-CoV-2. In response to other reviewers' comments, the authors have further improved the manuscript.

Reviewer #2

(Remarks to the Author)
I am satisfied by the response to my comments, the authors performed experiments that strengthen the conclusions of the study.

Reviewer #3

(Remarks to the Author)
In its revised version, the article by Mengxin Luo et al., “SARS-CoV-2 NSP14 inhibitor exhibits potent antiviral activity and reverses NSP14-driven host modulation”, addresses the vast majority of the reviewers’ comments. The additional information provided is important and strongly supports the conclusions of the study, which represents a preliminary step toward the development of antivirals targeting the SARS-CoV-2 N7-methyltransferase. I therefore recommend the publication of the revised manuscript in Nature Communications.

However, a few sentences remain incomplete or difficult to understand. I therefore recommend a careful proofreading of the manuscript prior to publication. Specific points that require correction include:

Lines 201–211: delete the expression “in the experimental end”.

Lines 310–311: the sentence “c10 did not disrupt the RNA capping but limits cap N7 methylation” is ambiguous and should be reformulated more clearly.

Lines 334–335: please clarify the expression “multiple antiviral effect”, which is currently difficult to understand.

Response to reviewers' comments

Luo et al. SARS-CoV-2 NSP14 inhibitor exhibits potent antiviral activity and reverses NSP14-driven host modulation

We sincerely appreciate the reviewers' insightful comments and constructive suggestions, which have significantly improved the quality of our manuscript. Below, we provide a point-by-point response to each reviewer's concern.

All revisions in the manuscript are highlighted as follows:

Reviewer #1: Red text

Reviewer #2: Blue text

Reviewer #3: Green text

The modifications made by the authors: Green background.

Reviewer #1 (Remarks to the Author):

Luo, et al, presented a non-nucleoside inhibitor of the SARS-CoV-2 NSP14 SAM-binding pocket, C10, which demonstrates robust antiviral activity against SARS-CoV-2, including its variants, comparable to remdesivir. And C10 could specifically reversed NSP14-mediated alterations in host transcriptome and restored host cell cycle progression disrupted by NSP14. This work pointed out the C10 as a promising candidate for the development of effective treatments against SARS-CoV-2 and its emerging variants and also uncovers a novel mechanism of NSP14 in SARS-CoV-2 pathogenesis and its therapeutic potential. It is a topic of interest to the researchers in the related areas but the paper needs very some improvement before acceptance for publication. My detailed comments are as follows:

We sincerely thank the reviewer for these constructive comments and are encouraged that our work may uncover the novel mechanism of NSP14 in SARS-CoV-2 pathogenesis and its therapeutic potential. We have carefully considered the feedback and made substantial revisions to address the concerns, which have significantly helped us improve the quality of our manuscript.

1.This work proposed that C10 can specifically bind in the SAM pocket of nsp14 and affect the capping process, thus inhibiting viral proliferation, but there are not enough biochemical experiments to prove that C10 inhibits the MTase of nsp14, and supplemental thin-layer chromatography analysis is recommended .Reference: Y. Chen, H. Cai, J. Pan, N. Xiang, P. Tien, T. Ahola, & D. Guo, Functional screen reveals SARS coronavirus nonstructural protein nsp14 as a novel cap N7 methyltransferase, Proc. Natl. Acad. Sci. U.S.A. 106 (9) 3484-3489, https://doi.org/10.1073/pnas.0808790106 (2009).

Response:

We appreciate the reviewer's suggestion regarding the need for additional biochemical validation of C10's inhibitory effect on MTase activity of NSP14. We have added thin-layer chromatography (TLC) analysis to the revised manuscript.

Under the optimized reaction conditions (0.1 mM SAM, 0.1 mM GpppG, 100 nM NSP14 in buffer 50 mM Tris-HCl, pH 8.0, 6 mM KCl, 2 mM DTT, and 1.25 mM $MgCl_2$), we observed that NSP14 efficiently converted SAM and GpppG to SAH and m7GpppG after 30 mins at 37°C. When 10 μM or 20 μM compound **C10** was added, the conversion was nearly abolished, demonstrating potent inhibition of NSP14's MTase activity. These results provide direct biochemical evidence that **C10** inhibits the MTase of NSP14, supporting our proposed mechanism of action.

We have incorporated these findings into the revised manuscript, and the revised figure is presented in **Extended Data Fig. 2d**.

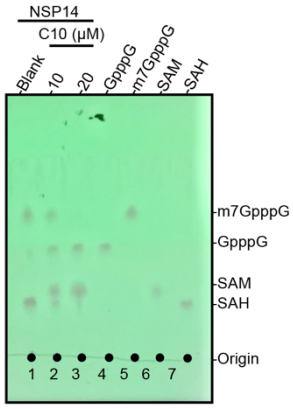

Extended Data Fig. 2d. TLC analysis of m7GpppG generated from GpppG and SAH generated from SAM after treatment with NSP14 (lanes 1–3). Addition of 10 μM or 20 μM C10 inhibited NSP14 activity, as shown in lanes 2–3. The migration positions of SAM, SAH, GpppG, and m7GpppG are indicated on the right.

The relevant text in the Results section have been updated as follows:

characterization and functional testing (**Fig. 1d**). To further evaluate C10's inhibitory effect on N7-MTase activity of NSP14, we conducted thin-layer chromatography (TLC) analysis of NSP14 N7-MTase activity in the presence of C10[13]. Treatment with C10 inhibited NSP14-mediated methylation in a dose-dependent manner, as evidenced by the dramatic reduction in m7GpppG formation and accumulation of unmetabolized SAM and GpppG (**Extended Data Fig. 2d**). These results demonstrate that C10 is a potent inhibitor of NSP14 N7-MTase, providing a biochemical basis for its potential antiviral effects.

2. Line 134-135: "The key residues for the binding of C10 to NSP14 predicted by the MM/GBSA free energy decomposition are listed in Fig. 2b." I think there is a clerical error. The key residues are listed in Fig. 3b.

Response:

We thank the reviewer for pointing this out. We apologize for the oversight and have corrected this clerical error in the revised manuscript.

3. Line 135-138: "The predicted structure of SARS-CoV-2 NSP14 bound to C10 and GpppG in a space-filling representation is shown in Fig. 3c. An expanded view of the bound C10 and GpppG (Fig. 3d) characterized a narrow binding pocket for C10, adjacent to the RNA cap-binding site."7BIF is a crystal structure of SARS-CoV-2 NSP14 in complex with 7MeGpppG instead of GpppG, and is similarly mislabeled in Fig. 3c, 3d and 3e.

Response:

We sincerely thank the reviewer for pointing out this important issue. The reviewer is correct that we mistakenly labeled "GpppG" instead of the correct "**m7GpppG**" in these panels. We apologize for the oversight and any confusion this may have caused.

To clarify, the molecular docking was not performed directly on the 7QIF structure. Instead, we used the crystal structure of the NSP14-SAH complex (PDB ID: 7R2V) as the docking template, with the SAH molecule removed to represent the apo structure of NSP14. The m7GpppG cap structure was modeled into the catalytic pocket based on the structural alignment with PDB ID **7QIF**, which served as a reference for cap-binding.

We have conducted a thorough review and carefully corrected all instances of this mislabeling in the revised manuscript.

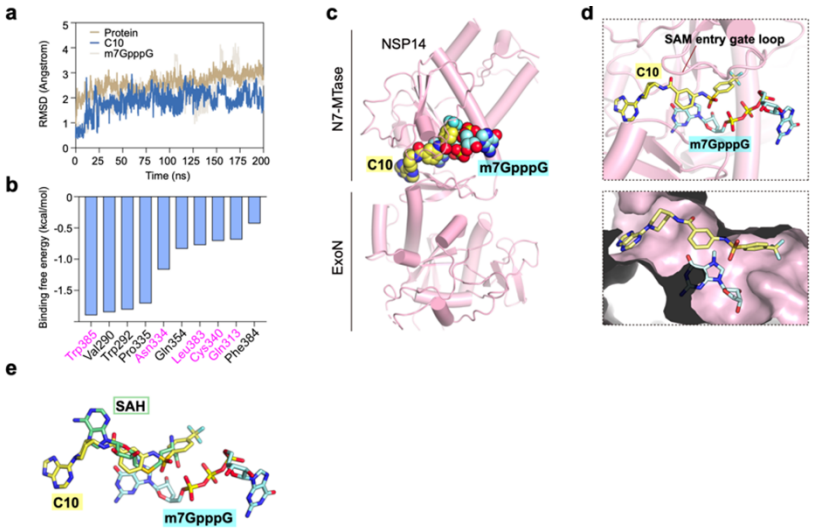

Extended Data Fig. 3a,c,d,e: The labels of "m7GpppG" have been revised accordingly.

4. Line 141-143: "First, the stronger electronegativity of the phenyl trifluoromethyl group in C10 provides additional electrostatic interactions with a druggable site (refers to site-C) composed of residues Arg310, Gln313, Asp331, Cys340, and Trp385."It would be useful to also label the interactions between fluoromethyl groups and site-C residues with a dashed line on Fig. 3g.

Response:

We thank the reviewer for this valuable suggestion. In response, we have revised **Figure 3g** to include dashed lines that explicitly depict the electrostatic interactions between the trifluoromethyl group (-CF_3) of C10 and the key residues comprising Site-C, namely Arg310, Gln313, Asp331, Cys340, and Trp385. This graphical enhancement improves the clarity of the proposed interaction network and facilitates a better structural understanding of C10's binding mode.

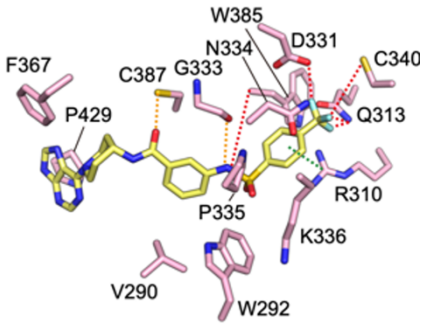

Fig. 3g. Key residues involved in the binding of C10 to NSP14. The red dashed lines represent hydrophobic interactions, the green dashed lines represent p-π conjugation, and the yellow dashed lines represent hydrogen bonding interactions.

To experimentally validate the contribution of Site-C residues to C10 binding, we generated a panel of NSP14 single-point mutants (W292R, R310A, Q313R, N334A, P335R, C340A, F384A, and W385A), focusing on those directly implicated in interactions with the CF_3 group based on our molecular docking analysis. Consistent with the computational predictions, all mutants exhibited reduced thermal shifts in differential scanning fluorimetry (DSF) assays (**Extended Data Fig. 8**). Notably, Q313R and W385A, both located within Site-C, showed the most significant decreases in ΔTm, supporting the proposed interaction network of revised **Fig. 3g**.

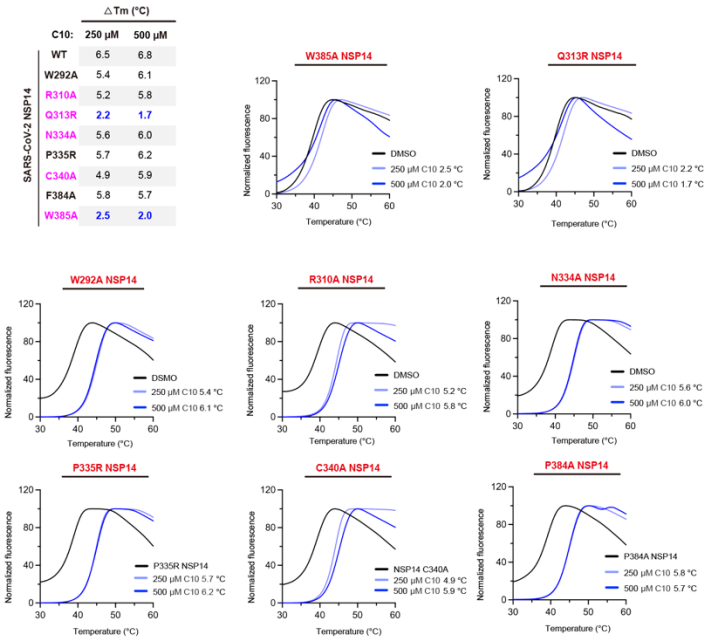

SARS-CoV-2 NSP14	ΔTm (°C) C10: 250 μM	500 μM
WT	6.5	6.8
W292A	5.4	6.1
R310A	5.2	5.8
Q313R	2.2	1.7
N334A	5.6	6.0
P335R	5.7	6.2
C340A	4.9	5.9
F384A	5.8	5.7
W385A	2.5	2.0

Extended Data Figure 8. Melting temperature shifts of SARS-CoV-2 NSP14 mutants by adding 250 μM and 500 μM C10, as measured by the DSF assays.

5.Line 232-233: "A Venn diagram analysis showed a significant overlap of the differentially expressed genes induced by NSP14 expression and those induced by NSP14 inhibition mediated by C10 (Fig. 5f)."In Fig. 5f, we can see the overlap of the upregulated genes induced by NSP14 expression and downregulated genes induced by C10, and vice versa. But, is there also an overlap between the upregulated genes induced by NSP14 expression and the upregulated genes after the induced by C10, or the downregulated genes induced by NSP14 expression and the downregulated genes after the induced by C10?

Response:

We thank the reviewer for bringing our attention to this point. After re-examining our RNA-seq data, we confirmed that there is no direct overlap between: genes upregulated by NSP14 expression and those upregulated by C10 treatment, or genes downregulated by NSP14 and those downregulated by C10 (**Fig. R1**). This pattern reinforces that NSP14 and its pharmacological inhibition by C10 exert functionally significant and opposing effects on host gene expression. All genes were listed in the source data.

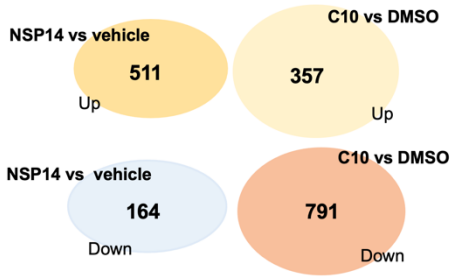

Fig. R1. Venn diagram illustrating the overlap of enriched genes between NSP14 vs vehicle and 20 μM C10 vs DMSO conditions. Data are presented as averages of two independent experiments.

Reviewer #2 (Remarks to the Author):

The manuscript describes the identification of a novel antiviral drug targeting the SARS-CoV-2 NSP14 N7-guanine-methyltransferase activity. A robust medicinal chemistry virtual screening approach followed by lead optimization identified the compound C10 for further characterisation. Biochemical/biophysical analysis confirmed the SAM pocked as the target and virtual SAR defined the involved residues in the pocket. Infection assays confirmed antiviral

activity in the low micromolar down to nanomolar for the Omicron variants, with a good SI. The compound is specific for Coronavirus MTase and more potent for SARS-CoV-2 than NCoV-OC43. They then show that C10 inhibits viral replication and reversed NSP14 modulation of the host transcriptome and NSP14 induced cell cycle arrest. Finally, they tested antiviral efficacy in vivo in the K18-hACE2 transgenic mouse model for SARS-CoV-2 infection. The importance of identifying novel targets for antiviral therapy of SARS-CoV-2, and viruses in general, is highlighted also by the recent work by Mayer et al (Nature 2025) demonstrating significant therapeutic potential of another inhibitor of NSP14 (TDI-015051) targeting the cap-binding site. Having two drugs effective for the same target with two different mechanisms might allow combination for next generation NSP14 inhibitors. While the medicinal chemistry approach appears robust, with extensive biochemical/biophysical characterisation, the biological/virological characterisation remains incomplete, below some specific considerations:

We sincerely thank the reviewer for the thoughtful comments regarding the biological and virological aspects of our study. We are encouraged that our work, alongside the compound TDI-015051 developed by Mayer et al. (*Nature*, 2025), may contribute to the development of next-generation NSP14 inhibitors. We have taken all feedback seriously, performed several additional key experiments, and made substantial revisions to the manuscript. We have outlined a revision to address the questions below.

- Data on virus inhibition start on Figure 4 with the analysis of different SARs-CoV-2 variants (lacks definition of strains, "original" is not sufficient). The experimental setup involves 1h pre-treatment with the drug prior to infection and readout at 24h. No time-of-addition experiments are shown. Activity on replication is confirmed with a replicon assay, which could be considered a surrogate test at best (Figure 5a, please use luciferase activity rather than RdRp activity). TOA is useful to understand also if the drug can act while the virus is replicating in vesicles.

Response:

1. Clarification of Virus Strain

We thank the reviewer for pointing this out. In the revised manuscript, we have replaced "original" with the defined strain name, **SARS-CoV-2 Wuhan-Hu-1**, which corresponds to the

reference strain used in our antiviral assays. The figures and the relevant text have been updated accordingly.

2. Time-of-Addition (TOA) Experiments

We appreciate the reviewer's insightful suggestion regarding **time-of-addition (TOA)** experiments to further elucidate the mechanism of action of C10. Accordingly, we performed TOA assays using SARS-CoV-2 virus-like-particles (trVLP) in A549-ACE2 cells. The SARS-CoV-2 trVLP system, comprising N gene-deleted genomic viral RNA and N protein-expressing producer cells, enables complete viral life cycle yet exclusively in cells ectopically expressing SARS-CoV-2 N protein, which has been previously characterized (Ju X, et al. *PLoS Pathogens*. 2021, PMC7990224; Yang B, et al. *Cell Discovery*. 2023, PMC10117269; Wang H, et al. *Science Advances*. 2024, PMC11305390) and provides a robust platform for studying viral replication inhibition while maintaining BSL-2 safety conditions.

Our results demonstrate that C10 exhibits potent antiviral activity when administered during full-time or post-entry phases but shows minimal inhibition when applied during the entry phase only. These findings suggest that C10 acts primarily at the post-entry replication stage, rather than inhibiting viral entry, consistent with its proposed mechanism as an NSP14 inhibitor (**Figure 4k**). These new data have been added to the revised manuscript as follows:

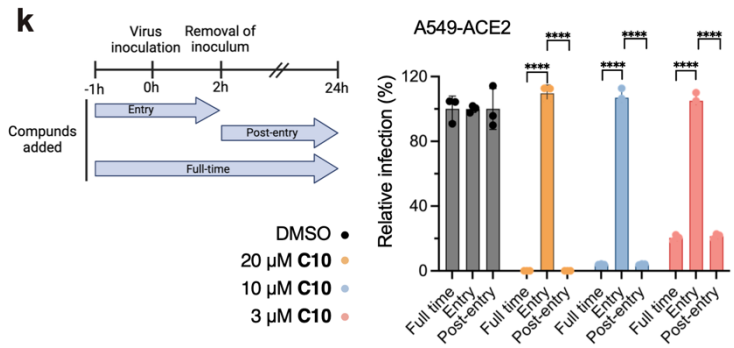

Fig. 4k. Time-of-addition analysis of C10. For all the experimental groups, cells were infected with SARS-CoV-2 trVLP at an MOI of 0.02, and the luciferase activity was measured. Data are presented as mean ± SD from three independent replicates. Statistical significance was determined by unpaired t-test, P****<0.0001.

Please see the updated paragraph below:

We next performed time-of-addition (TOA) experiments to further elucidate the mechanism of action of C10, using SARS-CoV-2 trVLP system in A549-ACE2 cells. C10 was treated at concentrations of 3 μM, 10 μM, and 20 μM during different stages of the viral life cycle: full-time treatment, entry phase, and post-entry phase (**Fig. 4k, left**). Our results show that C10 exhibits significantly stronger inhibitory activity during full-time and post-entry treatments, while minimal inhibition was observed when applied only during the entry phase (**Fig. 4k, right**). These findings suggest that C10 primarily targets the viral replication stage, consistent with its proposed mechanism of action as an NSP14 inhibitor.

3. Clarification of Readout in Replicon Assay

In response to the reviewer's suggestion, we have revised **Figure 4j** to describe the readout as **"Luciferase activity"** rather than "RdRp activity," to more accurately reflect the experimental setup. This adjustment ensures clarity while preserving the assay's intended role in assessing replication-phase inhibition by C10.

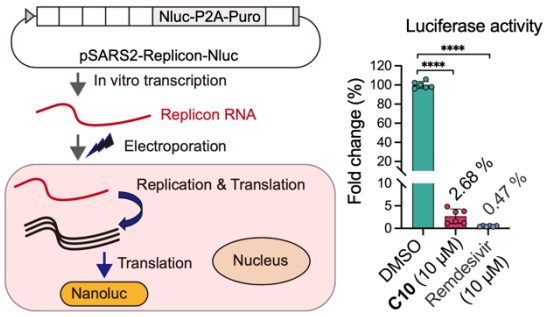

Fig. 4j. Schematic of the SARS-CoV-2 replicon assay (left) and quantification of replicon activity by luciferase reporter readout (right). Data are mean ± SD from three biological replicates. Statistical significance was determined by unpaired t-test; ****P < 0.0001.

- A critical experiment would be to select for resistant mutations by incubating cycles of virus infection with increasing concentrations of drug. This allows the identification of mutations in the target site of the drug and measurement of fitness of resulting viruses, all essential information for characterisation of a novel drug.

Response:

We sincerely thank the reviewer for this insightful suggestion. We fully agree with the importance of viral resistance selection experiments in identifying drug-target interactions and

evaluating the therapeutic potential of a novel compound. Below, we outline the modifications and additions made to address this comment.

1. Selection of resistant mutations

In response to the reviewer's suggestion, we conducted serial passaging of SARS-CoV-2 trVLP in Vero-N cells under increasing concentrations of **C10** to select **resistant mutations.** After five passages, we observed a gradual reduction in **C10**'s antiviral efficacy, indicating the emergence of drug-resistant variants (revised **Extended Data Fig. 11a,b)**. Next-generation sequencing (NGS) of the passaged viral populations revealed no significant mutations in NSP14 during the first two passages. However, by the third and fourth passages, we detected the emergence of V290A and P393L mutations in NSP14 at high frequencies. Notably, by the fifth passage, the V290A mutation reached a frequency of 96.73% (**Fig. 4i, Extended Data Fig. 11c**), suggesting strong positive selection under **C10** pressure.

Please see below the revised figures:

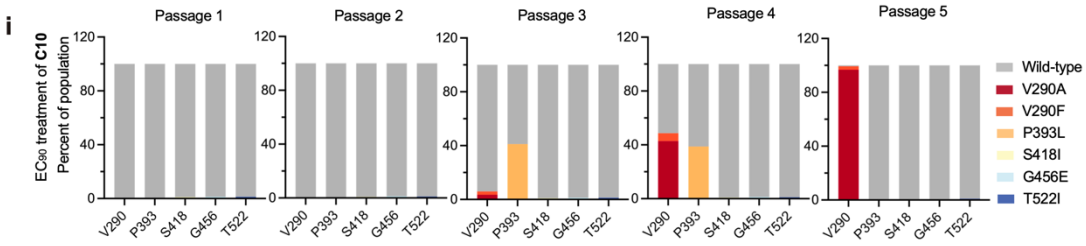

Fig. 4i. Frequency of NSP14 amino acid changes emerging in SARS-CoV-2 trVLP after 5 passages in Vero-N cells challenged with 10 μM or 20 μM C10.

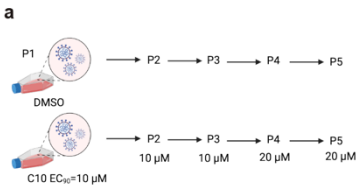

c

	Passage 1	Passage 2	Passage 3	Passage 4	Passage 5
V290A	0.01%	0.01%	3.42%	42.70%	96.73%
V290F	0.35%	0.38%	2.52%	5.95%	2.64%
P393L	0.05%	0.15%	41.16%	38.71%	0.10%
S418I	1.06%	0.85%	0.94%	0.85%	0.41%
G456E	1.20%	1.28%	1.19%	1.15%	0.44%
T522I	1.24%	1.05%	1.13%	1.06%	0.93%

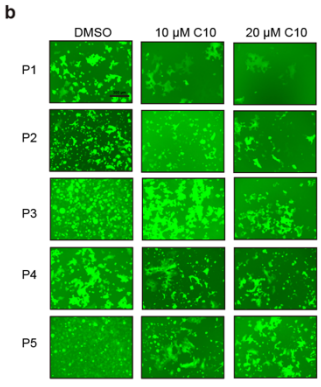

Extended Data Figure 11. Selection of resistance mutations and fitness competition assays. **a**. Schematic of the SARS-CoV-2 trVLP passaging protocol used to select for resistance mutations to C10 in Vero-N cells. **b**. Fluorescence images showing inhibition of C10-passaged viruses after each passage by treatment with 10 μM and 20 μM C10. **c**. Table summarizing the percentage of NSP14 amino acid changes emerging in SARS-CoV-2 trVLP populations.

We have incorporated these findings into the revised manuscript as follows:

Resistance mutations to compound C10

To identify resistance mutations and further elucidate the target site of compound C10, we conducted serial passaging under increasing concentrations of C10 by using the SARS-CoV-2 trVLP system, which consists of N gene-deleted genomic viral RNA and Vero-N cells[57–59]. This system enables completion of the full viral life cycle exclusively in cells expressing the SARS-CoV-2 N protein. After five passages, we observed a gradual reduction in C10's antiviral efficacy (**Extended Data Fig. 11a,b**), indicating the emergence of drug-resistant variants. Next-generation sequencing (NGS) of the passaged viral populations revealed no significant mutations in NSP14 during the first two passages. However, by the third and fourth passages, we detected the emergence of V290A and P393L mutations in NSP14 at high frequencies. Notably, by the fifth passage, the V290A mutation reached a frequency of 96.73%, suggesting strong positive selection under C10 pressure (**Fig. 4l**, **Extended Data Fig. 11c**).

2. Fitness Competition Assay of Resistant Mutants

We also followed the reviewer's suggestion to perform **fitness competition assays** by mixing wild-type and V290A SARS-CoV-2 trVLP at ratios of 10:0, 0:10, and 9:1, and passaging them for two rounds. NGS analysis revealed that, in the 9:1 mixture, wild-type NSP14 rapidly outcompeted the V290A mutant, with its proportion increasing to 94.34% after the first passage and reaching 100% after two passages (**Extended Data Fig. 11d**). This suggests that while the V290A mutation confers resistance under drug pressure, it significantly impairs viral fitness in the absence of **C10**.

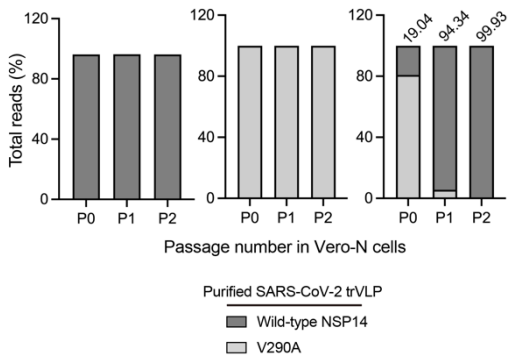

Extended Data Figure 11d. Assessment of viral fitness of wild-type and NSP14-V290A purified SARS-CoV-2 trVLP co-cultured starting at 10:0, 0:10, or 1:9 ratio monitored over 2 passages in A549-ACE2 cells, respectively.

We have incorporated these findings into the revised manuscript as follows:

We next performed fitness competition assays by mixing wild-type and V290A SARS-CoV-2 trVLP at ratios of 10:0, 0:10, and 9:1, and passaging them for two rounds. NGS analysis showed that in the 9:1 mixture, the wild-type NSP14 rapidly outcompeted the V290A mutant, with its proportion increasing to 94.34% after first passage, and reaching 100% after the two passages (Extended Data Fig. 11d). This suggests that the V290A mutation, although conferring resistance under drug pressure, reduces viral fitness in the absence of C10.

3. Functional relevance of identified resistant mutations

To validate the functional relevance of identified resistant mutations, NSP14 proteins bearing the V290A or P393L mutations were measured bindings to C10 in DSF assay. V290A and P393L mutants exhibited significantly reduced thermal stability (ΔTm=0.9 and 5.8°C) upon 250 μM C10 binding (**Extended Data Fig. 11e,f)**, compared to wild-type NSP14 (ΔTm=6.5 °C), indicating the critical role of these residues in C10 binding. Notably, the V290A mutation is consistent with our molecular simulation results, which highlight its direct involvement in the C10 binding interface (**Fig.3b**). In contrast, the P393L mutation resides outside the catalytic pocket and is embedded within the structural core of NSP14. We therefore hypothesize that P393L may influence C10 binding through an allosteric mechanism.

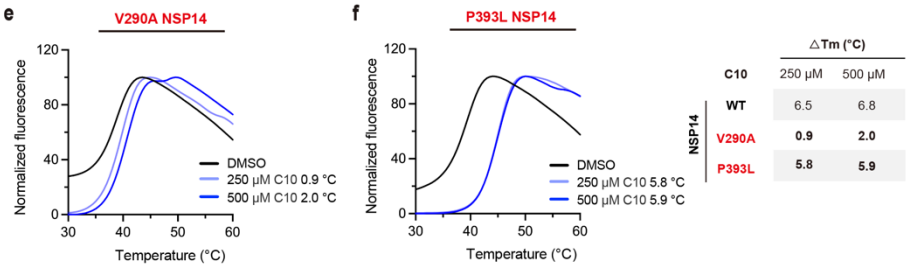

Extended Data Figure 11 e-f. Dose-dependent increase in melting temperature of NSP14 V290A and P393L mutants upon treatment with 250 μM and 500 μM C10, measured by DSF assay.

Please see the updated paragraph below:

To validate the functional relevance of identified resistant mutations, NSP14 proteins bearing the V290A or P393L mutations were measured bindings to C10 in DSF assay. V290A and P393L mutants exhibited significantly reduced thermal stability (ΔTm=0.9 and 5.8°C) upon 250 μM C10 binding (Extended Data Fig. 11e,f), compared to wild-type NSP14 (ΔTm=6.5 °C), indicating the critical role of these residues in C10 binding. Notably, the V290A mutation is consistent with our molecular simulation results, which highlight its direct involvement in the C10 binding interface (**Fig.3b**). In contrast, the P393L mutation resides outside the catalytic pocket and is embedded within the structural core of NSP14. We therefore hypothesize that P393L may influence C10 binding through an allosteric mechanism.

Taken together, these results identify V290 and P393 as critical residues mediating the binding of C10 to NSP14 and uncover a resistance mechanism involving the V290A substitution. While V290A confers resistance, its reduced fitness highlights a potential vulnerability that can be exploited in combination therapies or for the development of improved analogs. We have incorporated these findings and their therapeutic implications into the revised **Discussion** sections as below. We sincerely thank the reviewer for this important suggestion, which has significantly strengthened the depth and translational relevance of our study.

428 offering an opportunity for structure-guided drug design. Our results identify V290 and P393 as critical
429 residues involved in C10 binding to NSP14 and reveal a resistance mechanism driven by the V290A
430 substitution. Although the V290A mutation confers resistance, its reduced viral fitness highlights a
431 potential vulnerability that could be leveraged in combination therapies or for the development of
432 improved analogs.↵

- The direct outcome of inhibition of vRNA capping would be translation defects and generation of RNA that could trigger immune sensing and virus clearance. Neither of the two outcomes has been addressed.

Response:

We sincerely appreciate the reviewer's insightful comment regarding the translational and immunological consequences of C10 treatment. Addressing these outcomes provides crucial support for understanding the antiviral mechanism of C10.

1. Impact of C10 on viral mRNA translation

To evaluate the impact of C10 on mRNA translation, we performed polysome profiling of cell lysates using pre-treated A549-ACE2 cells with DMSO, 20 μM, or 40 μM C10, followed by infection with SARS-CoV-2 trVLP for 8 hours. Polysome profiling of cell lysates showed comparable overall profiles in the presence or absence of C10 (**Fig. 5a)**, indicating no global disruption of host translation. **To investigate whether C10 selectively impairs viral translation**, we assessed the abundance of SARS-CoV-2 Spike mRNA relative to host HPRT1 mRNA in different polysome fractions by RT-qPCR. Treatment with 20 μM and 40 μM C10 resulted in a 10-fold and 13-fold reduction respectively, compared to DMSO prior to polysome fractionation (**Fig. 5b, left**). Notably, this reduction was more significant in the heavy polysome fractions (~13-fold and ~40-fold for 20 μM and 40 μM C10, respectively) compared to the free polysome fractions (~2.5-fold and ~26-fold) (**Fig. 5b, right**), indicating impaired ribosome engagement with viral mRNA. These findings suggest that C10, by inhibiting NSP14 MTase activity, disrupts mRNA

capping, thereby selectively suppressing viral translation without broadly affecting host protein synthesis.

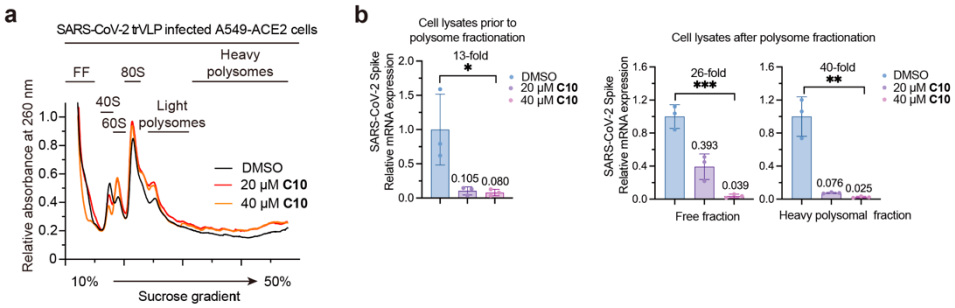

Fig. 5. a. Polysome profiling of SARS-CoV-2 trVLP infected A549-ACE2 cells treated with C10 (20 μM or 40 μM) or DMSO for 8 h, respectively. FF, free fraction. **b**. Left panel: Ratio of SARS-CoV-2 Spike mRNA relative to host HPRT1 in lysates of A549-ACE2 cells treated with C10 (20 μM or 40 μM) or DMSO and infected with SARS-CoV-2 trVLP for 8 h, respectively, prior to polysome fractionation. Right panel: Ratio of SARS-CoV-2 trVLP Spike mRNA relative to host HPRT1 in the free fraction or heavy polysomal fraction of lysates of A549-ACE2 cells treated with C10 (20 μM or 40 μM) or DMSO and infected with SARS-CoV-2 trVLP for 8 h, respectively, after polysome fractionation. n = 3; mean ± SD. Adjusted P values by ordinary one-way ANOVA are given. P * < 0.05; P ** <0.01; P *** <0.001.

2. C10 treatment exhibits immunostimulatory effect

To explore the immunostimulatory effects of C10 treatment, we measured the expression of several interferon-stimulated genes (ISGs), including RSAD2, IFI6, IRF7, IFIT2, and OAS1, in SARS-CoV-2 trVLP and A549-ACE2 cells system. In parallel, qPCR and western blot analyses confirmed that 20 μM C10 significantly reduced mRNA and protein expression of SARS-CoV-2 Spike, with remdesivir as a positive control (**Fig. 5c,d**). When compared to DMSO or Remdesivir, C10 treatment at 20 μM led to a modest increase in ISG expression (**Fig. 5e**), which is consistent with previously reported results of NSP14 inhibition by TDI-015051. These findings suggest that C10's inhibition of RNA capping triggers an immunostimulatory effect, which appears secondary to its primary antiviral effect. This immunological consequence likely contributes to the enhanced viral clearance observed with C10 treatment.

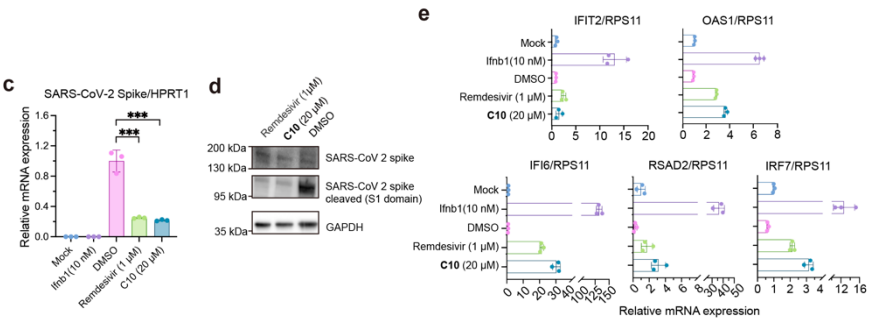

Fig. 5. c-d. Quantification of Spike expression by RT-qPCR (c) and western blotting (d) in SARS-CoV-2 trVLP infected A549-ACE2 cells treated with 20 µM C10. **e.** C10 inhibition of SARS-CoV-2 trVLP replication induces ISG expression in A549-ACE2 cells. Cells were mock-infected or infected with SARS-CoV-2 trVLP, pre-treated for 1 h with DMSO, C10 (20 µM), or remdesivir (1 µM), respectively; IFNB1 protein (10 nM) served as a positive control. Host and viral transcripts were quantified by RT-qPCR 24 h post-infection. Data are mean values from n = 3 biological replicates.

These results have been incorporated the revised manuscript as follows:

296 **C10 suppresses viral translation and exhibits immunostimulatory effect**

297 N7 methylation of the mRNA cap is critical for optimal recognition by eukaryotic translation initiation
298 factors, thereby supporting the translation of host and viral mRNAs. We performed polysome profiles of
299 mock-infected and VLP-infected cell lysates, which indicates that SARS-CoV-2 trVLP infection slightly
300 downregulated host translation (**Extended Data Fig. 12**). To further evaluate the impact of C10 on mRNA
301 translation, we pre-treated A549-ACE2 cells with DMSO, 20 µM, or 40 µM C10, followed by infection with
302 SARS-CoV-2 trVLP for 8 hours. Polysome profiling of cell lysates showed comparable overall profiles in
303 the presence or absence of C10 (**Fig. 5a**), indicating no global disruption of host translation. To
304 investigate whether C10 selectively impairs viral translation, we assessed the abundance of SARS-CoV-2
305 Spike mRNA relative to host HPRT1 mRNA in different polysome fractions by RT-qPCR. Treatment with
306 20 µM and 40 µM C10 resulted in a 10-fold and 13-fold reduction respectively, compared to DMSO prior
307 to polysome fractionation (**Fig. 5b, left**). Notably, this reduction was more significant in the heavy
308 polysome fractions (~13-fold and ~40-fold for 20 µM and 40 µM C10, respectively) compared to the free
309 polysome fractions (~2.5-fold and ~26-fold) (**Fig. 5b, right**), indicating impaired ribosome engagement
310 with viral mRNA. These findings suggest that C10, by inhibiting NSP14 MTase activity, disrupts mRNA
311 capping, thereby selectively suppressing viral translation without broadly affecting host protein synthesis.

312 To explore the immunostimulatory effects of C10 treatment, we measured the expression of
313 several interferon-stimulated genes (ISGs)[44,61], including RSAD2, IFI6, IRF7, IFIT2, and OAS1, in
314 SARS-CoV-2 trVLP and A549-ACE2 cells system. In parallel, qPCR and western blot analyses confirmed
315 that 20 µM C10 significantly reduced mRNA and protein expression of SARS-CoV-2 Spike, with
316 remdesivir as a positive control (**Fig. 5c,d**). When compared to DMSO or Remdesivir, C10 treatment at 20
317 µM led to a modest increase in ISG expression (**Fig. 5e**), which is consistent with previously reported
318 results of NSP14 inhibition by TDI-015051[44]. These findings suggest that C10's inhibition of RNA capping
319 triggers an immunostimulatory effect, which appears secondary to its primary antiviral effect. This
320 immunological consequence likely contributes to the enhanced viral clearance observed with C10
321 treatment.

- Instead, the authors engage in an analysis of the effect of the drug on indirect activities of NSP14 on the cell transcriptome and cell cycle. It took me some time to understand if the MTase activity of NSP14 was required and maybe it could be useful if the authors mention this in the

text and the associated reference (Zaffagni et al. eLife 2022). Discussion could include also the role of IMPDH2 as NSP14 associated protein also required for the global effect on gene expression.

Response:

We thank reviewer for pointing this out. We have added a description in the revised manuscript to highlight a previous report by Zaffagni et al. (*eLife*, 2022), which established that the MTase activity of NSP14 is required for host transcriptome modulation. This addition helps to contextualize our findings within the existing framework of NSP14's role in regulating host gene expression.

> Among all SARS-CoV-2 non-structural proteins, NSP14 has been uniquely shown to induce extensive remodeling of the host transcriptome, closely resembling the alterations observed during SARS-CoV-2 infection[15]. Additionally, NSP14 expression led to changes in the splicing of over 1,000 genes, implicating a pathogenic role that extends beyond its canonical function in viral RNA capping. Notably, these transcriptomic and splicing effects are independent of the ExoN domain but require an intact N7-MTase domain[15]. We infer that small-molecule inhibition of NSP14 methyltransferase, as achieved by C10, could reverse NSP14-driven host transcriptome modulation.

As suggested, we investigated the role of IMPDH2, a host protein associated with NSP14 and implicated in global transcriptomic regulation, as highlighted in previous work by Zaffagni et al. (*eLife*, 2022). Guanosine triphosphate (GTP) levels inversely regulate inosine monophosphate dehydrogenase 2 (IMPDH2) expression, and NSP14 has been shown to activate IMPDH2, elevating GTP levels and thereby suppressing IMPDH2 mRNA expression. Consistent with this mechanism, our RNA-seq and RT-qPCR analyses confirmed that NSP14 expression reduced IMPDH2 transcript levels (**Fig. 5l,m**). C10 treatment dose-dependently restored IMPDH2 mRNA levels (**Fig. 5l,m**), supporting the conclusion that C10 counteracts NSP14-mediated downregulation of IMPDH2. These findings reinforce the mechanistic link between NSP14 and host transcriptome modulation. We have incorporated these new results into the revised manuscript as follows:

> Several of the most enriched genes overlapped with those reported in the previous study, such as *CREBBP* and *Z3CH4*[15] **(Extended Data Fig. 13b, c)**. Guanosine triphosphate (GTP) levels inversely regulate inosine monophosphate dehydrogenase 2 (IMPDH2) expression, and NSP14 has been shown to activate IMPDH2, elevating GTP levels and thereby suppressing *IMPDH2* mRNA expression[23,62]. Consistent with this mechanism, our RNA-seq and RT-qPCR analyses confirmed that NSP14 expression reduced *IMPDH2* transcript levels (**Fig. 5l,m**). C10 treatment dose-dependently restored *IMPDH2* mRNA levels (**Fig. 5l,m**), supporting the conclusion that C10 counteracts NSP14-mediated downregulation of IMPDH2.

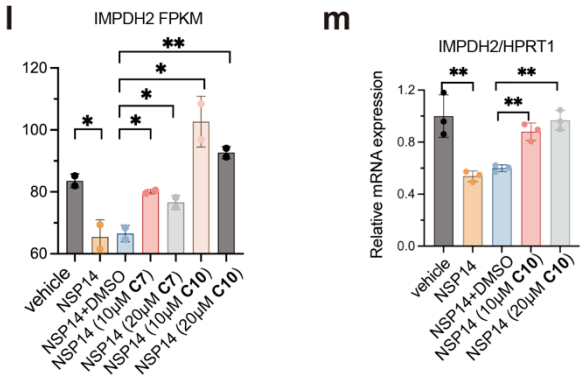

Fig. 5. l. FPKM analysis of *IMPDH2* from RNA-seq data. Data are presented as averages of two independent experiments. **m.** *IMPDH2* transcriptional changes as detected by qPCR. Data are presented as mean ± SD from three replicates. Statistical significance was analyzed by unpaired t-test. P****<0.0001.

- In vivo experimentation is welcome. However, more discussion of the results is needed. For example, Figure 6f shows non-significant reduction of virus titre in lungs at non-toxic concentrations (<100 mg/kg) indicating more work to optimise this class of inhibitors in vivo to reduce toxicity and increase efficacy. Figure 6j shows similar decrease of N antigen staining compared to Remdesivir control but at higher concentrations (120 mg/kg). To conclude, although the results are promising, still the drug would require further optimisation for successful in vivo administration. Furthermore, a more accurate virological analysis would be helpful also for optimisation (i.e. binding site mutations).

Response:

We thank the reviewer for highlighting the importance of critically assessing the in vivo data and recognizing the need for further optimization of this compound class. As correctly noted, while administration of C10 at 120 mg/kg led to a reduction in lung viral titers and N antigen staining comparable to that observed with 20 mg/kg remdesivir (**Fig. 6f, 6j**), the lower dose of 60 mg/kg failed to produce a statistically significant antiviral effect. These findings suggest that, although C10 exhibits in vivo efficacy, its current therapeutic window remains narrow and further medicinal chemistry efforts are required to enhance potency, reduce toxicity, and improve pharmacokinetic properties. We have revised the **Result** and **Discussion** section to clearly acknowledge these limitations and emphasize the need for future optimization to advance C10 or related analogs toward clinical development.

Result section:

mice had significantly lower lung viral titers (mean titer of Log10 PFU/g = 4.99, P < 0.05) (**Fig. 6f**). Mice treated with 60 mg/kg C10 showed reduced lung viral titers compared to vehicle-treated controls, though the difference was not statistically significant (**Fig. 6f**). These results highlight the need for further structural optimization of these inhibitors.

Discussion section:

Our current findings provide preliminary proof-of-concept that NSP14 inhibition exhibits multiple antiviral effects. However, the effective dose of C10 is approximately eight-fold higher than that of remdesivir, indicating substantial medicinal chemical modification will be required to improve the therapeutic index before clinical translation. Future medicinal chemistry efforts will focus on further optimizing the pharmacokinetic properties of C10 while maintaining its high potency and selectivity.

As also recommended, to better understand the drug-target interaction and inform structure-based optimization, we performed serial passaging of SARS-CoV-2 trVLP under increasing C10 concentrations. This led to the identification of a resistance-associated V290A mutation in NSP14. Differential scanning fluorimetry (DSF) confirmed that the V290A mutant exhibited markedly reduced binding affinity to C10, providing direct biochemical evidence of target engagement and further validating the proposed binding interface. These mechanistic insights offer valuable direction for rational design of improved analogs with enhanced resistance profiles. We sincerely thank the reviewer for these constructive suggestions, which have significantly strengthened translational relevance of our in vivo and drug development discussions.

Reviewer #3 (Remarks to the Author):

The circulation of SARS-CoV-2 in the human population, the occurrence of chronic infections in immunocompromised individuals or in some patients with long COVID, and the emergence of variants resistant to the limited antiviral treatments currently available all underscore the urgent need for new, effective antiviral strategies against coronaviruses. In this study, the authors identify inhibitors of the N7-methyltransferase (MTase) activity of the nsp14 protein, which is involved in synthesizing the cap structure essential for the translation of viral messenger RNAs into proteins. Inhibition of this enzyme class using analogs of the methyl donor S-adenosylmethionine (SAM, an adenosine derivative) has already been explored by several groups, leading to the identification of selective inhibitors active, in vitro, in the nanomolar

range (10–500 nM). However, most of these compounds have shown limited efficacy in infected cells. In the present study, the inhibitors target the same catalytic pocket but are not nucleoside analogs. Using this approach, the authors identified compounds active both in vitro and in infected cells, with EC50 values ranging from 64 to 301 nM. Some antiviral efficacy was also demonstrated in a mouse model of SARS-CoV-2 infection, although the compounds appear toxic at higher doses (2,5x). Furthermore, the candidate molecules exhibit antiviral activity against multiple SARS-CoV-2 variants and prevent transcriptome remodelling observed in infected cells. Overall, this study is well-designed and provides substantial preliminary data that may contribute to the development of new antiviral strategies against this virus family. However, while the findings are important for the field of antiviral drug development, several conclusions are not fully supported by the experimental data, and additional experiments are needed before publication in Nature Communications.

We sincerely thank the reviewer for the thorough evaluation of our study and the detailed feedback. We are grateful that our well-designed work is recognized as providing substantial preliminary data that may contribute to the development of novel antiviral strategies targeting the coronavirus family.

Major Comments

1.Clarification of the Mode of Action of Compound C10

The abstract, the end of the introduction, and paragraph 3 ("C10 directly inhibits the genomic replication of SARS-CoV-2") suggest a direct inhibition of viral replication by C10. However, the data presented do not support a direct effect on the viral replication machinery. Direct inhibition would imply an interaction with the viral polymerase complex, which is not demonstrated here. Instead, the compound more likely targets viral mRNA translation and modulates host transcriptome responses via an unknown mechanism. The most plausible hypothesis is that C10 interferes with viral protein synthesis, thereby limiting the production of replication complexes and in turn will modulates the replication. This hypothesis could be experimentally confirmed by analyzing C10's effect on viral protein expression levels.

Response:

We thank the reviewer for this important and insightful comment regarding the mechanistic interpretation of C10's antiviral activity. We fully agree that the current data do not support a direct interaction between C10 and the viral RNA-dependent RNA polymerase

complex. In response, we have carefully revised the manuscript to avoid overinterpretation of C10's mode of action. Specifically, the original phrasing "C10 directly inhibits the genomic replication of SARS-CoV-2" has been updated to "**C10 inhibits SARS-CoV-2 at the replication stage**" to provide a more accurate description.

To further clarify whether C10 impacts viral replication indirectly by interfering with viral protein synthesis, we conducted additional mechanistic studies focusing on its effect on mRNA translation. **Polysome profiling** of SARS-CoV-2 trVLP infected A549-ACE2 cells pre-treated with DMSO, 20 μM, or 40 μM C10 revealed comparable global translation profiles across all conditions (**Fig. 5a**), suggesting that C10 does not impair overall host protein synthesis. However, RT-qPCR analysis of viral Spike mRNA relative to host HPRT1 mRNA showed a marked, dose-dependent reduction in viral RNA abundance (~10- and ~13-fold for 20 μM and 40 μM C10, respectively) prior to polysome fractionation (**Fig. 5b, left**). Notably, this reduction was even more obvious in the heavy polysome fractions (~13- and ~40-fold), which represent actively translating ribosomes, compared to the free polysome fractions (~2.5- and ~26-fold) (**Fig. 5b, right**), indicating compromised ribosome engagement with viral mRNAs.

In parallel, both qPCR and western blot analyses confirmed that 20 μM C10 significantly reduced the mRNA and protein levels of SARS-CoV-2 Spike, comparable to remdesivir (**Fig. 5c,d**), thereby further supporting a block in viral protein production. Taken together, these findings are consistent with a mechanism in which C10 targets NSP14's N7-MTase activity, disrupting viral mRNA capping, selectively impairing translation of viral transcripts, and thereby limiting downstream replication events such as replication complex formation.

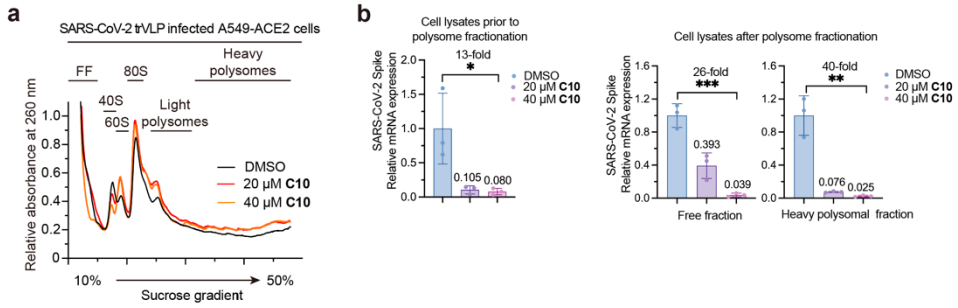

Fig. 5. a. Polysome profiling of SARS-CoV-2 trVLP infected A549-ACE2 cells treated with C10 (20 μM or 40 μM) or DMSO for 8 h, respectively. FF, free fraction. **b**. Left panel: Ratio of SARS-CoV-2 Spike mRNA relative to host HPRT1 in lysates of A549-ACE2 cells treated with C10 (20 μM or 40 μM) or DMSO and infected with SARS-CoV-2 trVLP for 8 h, respectively, prior to polysome fractionation. Right panel: Ratio of SARS-CoV-2 trVLP Spike

mRNA relative to host HPRT1 in the free fraction or heavy polysomal fraction of lysates of A549-ACE2 cells treated with C10 (20 µM or 40 µM) or DMSO and infected with SARS-CoV-2 trVLP for 8 h, respectively, after polysome fractionation. n = 3; mean ± SD. Adjusted P values by ordinary one-way ANOVA are given. P * < 0.05; P ** <0.01; P *** <0.001.

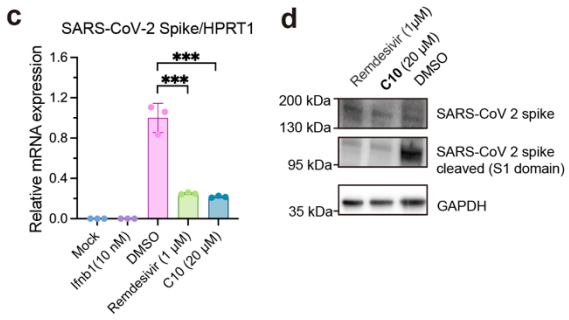

Fig. 5. c-d. Quantification of Spike expression by RT-qPCR (c) and western blotting (d) in SARS-CoV-2 trVLP infected A549-ACE2 cells treated with 20 µM C10.

2. Figure 1–ExoN Activity Control

It is important to demonstrate that compounds C3 and C10 do not affect the ExoN activity of nsp14, either in the presence or absence of its co-factor nsp10. This would clarify that the compounds specifically target the N7-MTase activity.

Response:

We thank the reviewer for highlighting this important point regarding the enzymatic specificity of C10 and related compounds. To address this, we conducted additional experiments to determine whether compounds C3 and C10 affect the 3′-5′ exonuclease (ExoN) activity of NSP14, in the presence of its cofactor NSP10.

ExoN activity assays were performed using purified NSP14-NSP10 complexes, with a synthetic double-stranded RNA (dsRNA) substrate as previously described (Rona et al., *Cell Death Differ* 2022, PMC8640510). We first optimized assay parameters by titrating dsRNA (50, 100, and 200 nM) and enzyme complex concentrations to achieve maximal substrate turnover and signal-to-noise ratio. Based on this optimization, subsequent assays were performed using 100 nM dsRNA and 195.8 nM NSP14-NSP10 complex (**Extended Data Fig. 2g**).

Under these conditions, neither compound C3 nor C10, at concentrations up to 200 µM, exhibited any detectable inhibition of ExoN activity (**Fig. 1j**). These findings indicate that both

compounds do not interfere with the ExoN function of NSP14 and suggest that their antiviral activity is specific to inhibition of the N7-MTase domain.

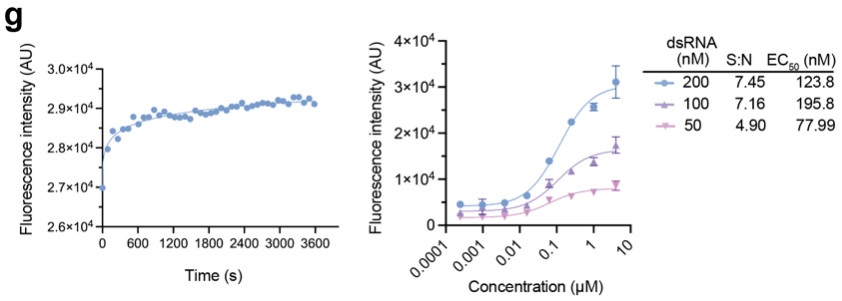

Extended Data Fig. 2g. Time-dependent NSP14-NSP10 exonuclease activity curves measured by the FRET assay (left). NSP14-NSP10 concentration-dependent exonuclease activity curves with 50 nM, 100 nM, and 200 nM dsRNA substrate (right).

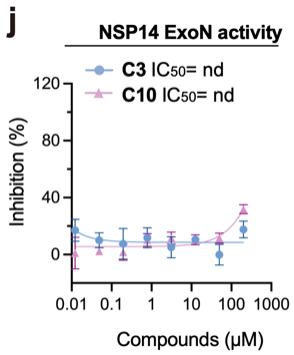

Fig. 1j. Dose-response inhibition curves of C3 and C10 against the NSP14-NSP10 complex, measured by the FRET-based exonuclease assay. Data are mean ± SD from three independent replicates.

We believe these results further strengthen the mechanistic conclusions of our study by confirming the domain-specific inhibitory action of C10 on NSP14.We have included these new data into the revised manuscript as follows:

130 examined whether C-family compounds interfere with the ExoN activity of NSP14. Using an exonuclease
131 assay with the purified NSP14-10 complex[52], neither C3 nor C10 inhibited ExoN activity (Fig. 1j ,
132 Extended Data Fig. 2g). These results demonstrate that C-family compounds selectively inhibit the
133 N7-MTase activity of NSP14 without affecting its ExoN function, thereby supporting their mechanism as
134 highly specific methyltransferase inhibitors.

3. Figure 2 – puzzling experimental design of figure 2.

Figure 2 lacks consistency. In some panels (e.g., 2B and 2H), GpppG is used, while in others (e.g., 2D), m7GpppG is tested. For robust interpretation, both analogs (GpppG and m7GpppG) as well as SAH should be tested across all relevant assays (DSF, SPR).

Response:

We thank the reviewer for pointing this out. We fully agree that including all relevant analogs (including GpppG, m7GpppG, SAM, and SAH) across both DSF and SPR experiments would enhance the interpretability of our data.

To address this concern, we conducted additional competitive binding assays using all relevant ligands across both DSF and SPR experiments. In the SPR assays, 20 µM SAH completely abolished C10's binding to NSP14, confirming that C10 competes at the SAH binding site (**Extended Data Fig. 6a**). In contrast, 20 µM m7GpppG had no effect on C10 binding, indicating a distinct and non-overlapping binding site (**Extended Data Fig. 6b**). In DSF assays, the addition of 200 µM GpppG to C10 at 20 µM, 250 µM, and 500 µM concentrations resulted in ΔTm increases of 10.9 °C, 11.2 °C, and 13.2 °C, respectively, further confirming the non-competitive nature of C10's binding with respect to the cap analog substrates (**Fig. 2f**). These new data are consistent with our existing results and further support our understanding of C10 as a SAM/SAH-competitive inhibitor.

For clarity, we have included all the data involving **GpppG** and **SAM** in revised **Figure 2**, as they are most directly relevant to the proposed mechanism of action., while the product **SAH** and **m7GpppG** competition assays are now included in the **Extended Data Fig. 4 and 6**.

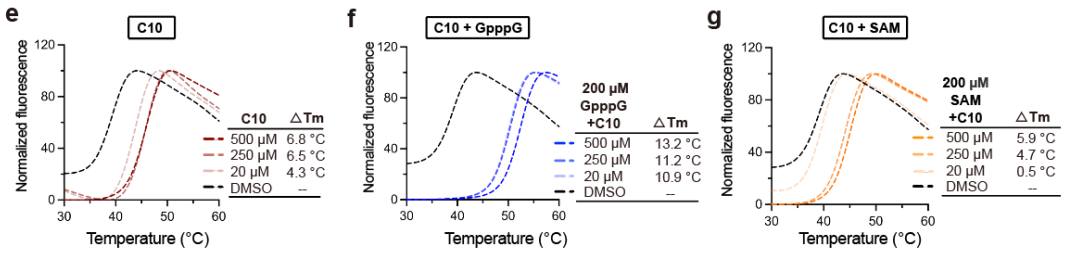

Fig.2f-g. In the presence of 200 µM GpppG (f), instead of 200 µM SAM (g), treatment with C10 caused an additional increase in the Tm of NSP14, exhibiting a synergistic effect between C10 and GpppG.

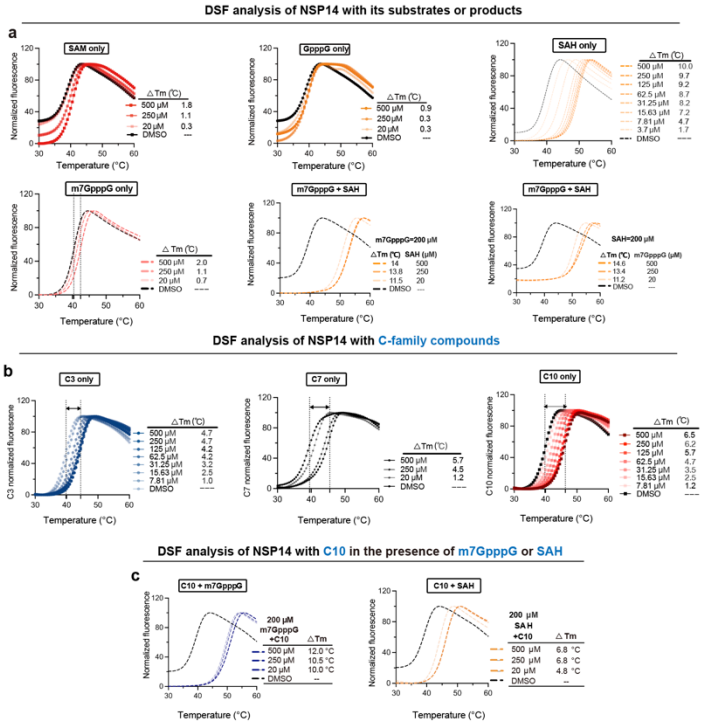

Extended Data Fig. 4a. DSF analysis of NSP14 in the presence of its substrates (SAM and GpppG), products (SAH and m7GpppG), and the product combination (SAH + m7GpppG). **c**. In the presence of 200 µM m7GpppG, instead of 200 µM SAH, treatment with C10 caused an additional increase in the Tm of NSP14, exhibiting a synergistic effect between C10 and m7GpppG.

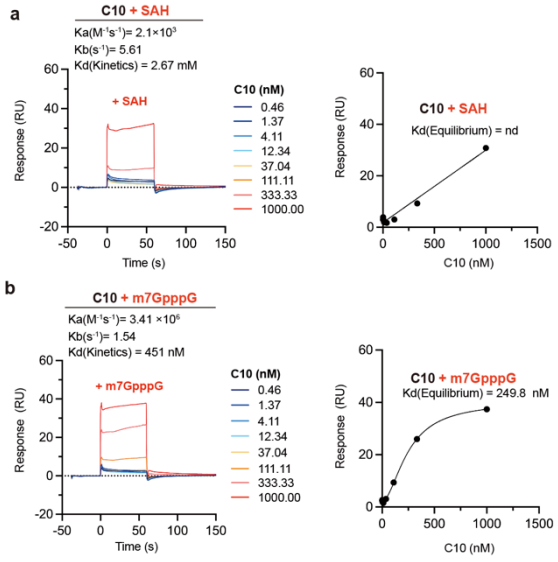

Extended Data Fig. 6. SPR binding assays for NSP14 and C10 in the presence of SAH or m7GpppG. SPR binding data indicating that the binding affinity of C10 with immobilized NSP14 is reduced in the presence of SAH (a) compared to m7GpppG (b), suggesting a SAH-

competitive binding mode.

4. Structural Modeling and Validation of C10 Binding

The authors present a structural model of C10 bound in the SAM-binding pocket of nsp14 and offer indirect evidence of specific binding. However, crystallization of full-length nsp14 appears unsuccessful. Recent studies (PMID: 36075969, 39188530) have shown that the isolated MTase domain can be crystallized when fused with a TELSAM tag. This construct could be used to attempt co-crystallization with C10, providing direct structural confirmation.

Response:

We sincerely appreciate the reviewer's constructive suggestion regarding the potential utility of the TELSAM-tagged NSP14 MTase domain for co-crystallization studies with C10. Indeed, prior to our initial submission, we conducted extensive crystallization screening using the TELSAM-tagged NSP14 MTase domain alone and in complex with SAH or C10 (**Fig. R2**). Despite exhaustive efforts, we were unable to obtain crystals with sufficient diffraction quality.

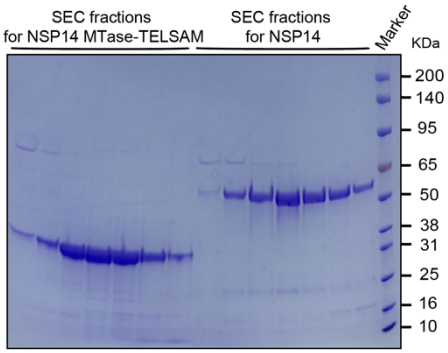

Fig. R2. SDS-PAGE result of the purified NSP14 related protein samples used for crystallization trials.

Given these technical challenges, and encouraged by the reviewer's suggestion, we have now conducted hydrogen-deuterium exchange mass spectrometry (**HDX-MS**) as an alternative approach to gain structural insights into the C10-NSP14 interaction. This technique monitors changes in amide hydrogen exchange rates upon ligand binding, thereby revealing conformational dynamics and putative binding sites at the peptide level. In this method, regions of the protein with decreased deuterium incorporation upon ligand binding are generally considered to be involved in direct interaction or allosteric conformational stabilization (**Extended Data Fig. 9**).

Our HDX-MS analysis revealed significant deuterium uptake changes in several key

peptides upon C10 binding (**Fig. 3k,l**): peptides 385-396, 303-318, and 338-347, which located in SITE-C, showed decreased deuterium incorporation by 4.88%, 2.32%, and 6.02%. Respectively, the reduction indicated substantial interactions involving the trifluoromethyl group with surrounding residues Q313, W385, and C340, consistent with our molecular dynamics simulations. Notably, peptide 287-295 exhibited the most pronounced interaction with 8.79% decrease, suggesting close proximity to the sulfonamide moiety. Also, peptide 351-367 showed 6.02% decreased deuterium exchange rate, consistent with interactions involving the pyrimidoimidazole ring. Interestingly, peptide 323-344 displayed increased deuterium incorporation, likely reflecting conformational adjustments near the beta-sheet region where our simulations predicted a hydrogen bond between G333 and the sulfonamide group. These comprehensive HDX-MS results, corroborated by molecular dynamics simulations, provide robust experimental evidence for C10 binding interactions with the NSP14 MTase domain. While we acknowledge that crystal structures remain the gold standard, our multi-technique approach offers complementary dynamic and structural insights into the C10 binding mechanism.

k

Peptide	% Deut change at 10s	at 60s	at 600s
287-295	-1.51	3.67	8.79
303-318	-0.13	0.69	2.32
323-344	-1.75	0.31	-3.82
338-347	-1.32	1.08	6.02
351-367	-1.40	2.32	6.20
385-396	-0.45	2.76	4.88

l

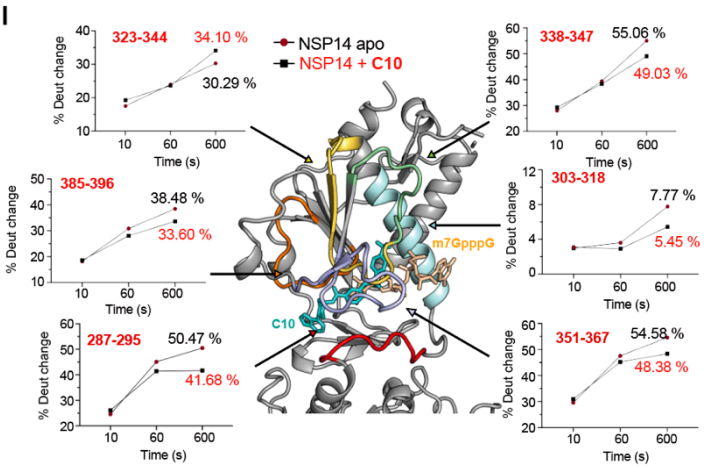

Fig. 3k. The change of deuterium exchange rate is shown for six representative fragments after C10 binding at three time points corresponding to 10, 60 and 600 s. **l**. Regions of H/D exchange most affected by C10 binding to NSP14. The deuterium exchange rate is shown for six representative fragments in the presence (black squares) and absence (red circles) of C10. The black and red curves indicate the rate of H/D exchanges at three time points corresponding to 10, 60 and 600 s. Compound refers to C10.

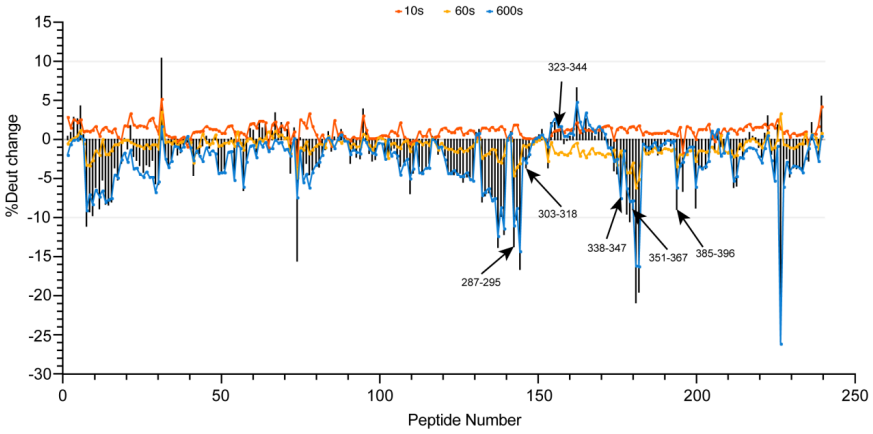

Extended Data Fig.9. General summary of Hydrogen-Deuterium Exchange Mass Spectrometry, Line chart for the change of deuterium exchange rate is shown for all fragments after C10 binding at three time points corresponding to 10, 60 and 600 s. The bar chart represents the accumulation of the change of deuterium exchange rate for all fragments after C10 binding at 10, 60 and 600 s. %Deut change = %Deut (NSP14-C10) - %Deut (NSP14 apo).

We believe these results further enhance the SAR understanding in our study by experimentally confirming the binding pocket of C10 on NSP14. We have incorporated these new data into the revised manuscript as follows:

To further gain structural insights into the C10-NSP14 interaction in the experimental end, we conducted hydrogen-deuterium exchange mass spectrometry (HD-MS) analysis. Several peptide regions of NSP14 revealed significant changes in deuterium uptake upon C10 binding, as illustrated by differences in hydrogen-deuterium exchange rates at various time points (**Extended Data Fig. 9**). Peptides 385-396, 303-318, and 338-347, corresponding to Site-C, showed reduced deuterium incorporation by 4.88%, 2.32%, and 6.02%, respectively **(Fig. 3k,l)**, suggesting interactions between the trifluoromethyl group of C10 and surrounding residues such as Gln313, Trp385, and Cys340. Peptide 287-295 exhibited the greatest reduction in deuterium uptake (8.79%), pointing to strong interactions with the sulfonamide moiety. Similarly, peptide 351-367, overlapping with the SAM/SAH interacting loop, showed a 6.02% reduction, consistent with binding of the pyrimidoimidazole ring. Interestingly, peptide 323–344 demonstrated increased deuterium exchange, likely reflecting localized conformational changes near the β-sheet region **(Fig. 3k,l)**. Consistent with the molecular dynamics simulation results, the HDX-MS data provide experimental evidence for the predicted binding mode of C10 within the catalytic pocket of the NSP14 MTase domain.

5. Functional Analysis of Mutants

Mutational analysis indicates that Q313R and W385A are involved in C10 binding. It would be valuable to assess whether additional mutations in site-C also impact C10 binding. Moreover,

it should be determined whether these mutations alter N7-MTase activity and confer resistance to C10 in a viral context. If enzymatic function is impaired, an alternative approach could be to select C10-resistant viral mutants to validate the binding model and assess the impact of these mutations on biophysical readouts (DSF, SPR). These studies would help evaluate the resistance potential of this compound class.

Response:

We sincerely thank the reviewer for their insightful comments regarding the binding specificity and resistance potential of C10.

To further **validate the key residues involved in C10 binding on NSP14,** we performed DSF assays using a panel of single-point mutants, including W292R, R310A, Q313R, N334A, P335R, C340A, F384A, and W385A. Compared to wild-type (WT) NSP14, which showed ΔTm shifts of 6.5 °C and 6.8 °C upon treatment with 250 and 500 µM C10 respectively, all mutants exhibited reduced thermal stabilization (**Fig. 3h**). Notably, Q313R and W385A, located in the defined Site-C, displayed the greatest reduction in ΔTm (2.2 °C and 2.5 °C, respectively; **Fig. 3h, Extended Data Fig. 8**), suggesting the impact of these residues for C10 interaction.

To assess **whether mutations Q313R and W385A affect the enzymatic activity of NSP14**, we conducted MTase-Glo assays. Both Q313R and W385A mutants retained catalytic activity comparable to WT NSP14, with only moderate changes in Km values (WT: 254.4 nM; Q313R: 463.5 nM; W385A: 729.7 nM), and showed no significant differences in maximal enzymatic output (**Fig. 3i**). These results indicate that these mutations do not compromise the intrinsic enzymatic function of NSP14.

In contrast, the inhibitory potency of C10 was markedly diminished in these mutants. The IC_{50} for C10 increased from 376.1 nM in WT NSP14 to >50 µM (Q313R) and 49.79 µM (W385A) (**Fig. 3j**), strongly indicating that Q313 and W385 are essential for C10 binding but not for enzymatic function. Together with the DSF data, this provides strong evidence that C10 directly engages Site-C and that these residues mediate compound binding.

To further explore the resistance potential of C10 in a viral context, we performed SARS-CoV-2 trVLP resistance evolution experiments under compound pressure. As detailed in our response to Reviewer 2, serial passaging led to the emergence of a resistance-associated mutation (V290A) only at later passages (P4–P5), highlighting a relatively high genetic barrier to resistance. Importantly, V290 also maps to the binding site in our predicted model (**Fig3b,g**), reinforcing the functional relevance of C10 binding mode.

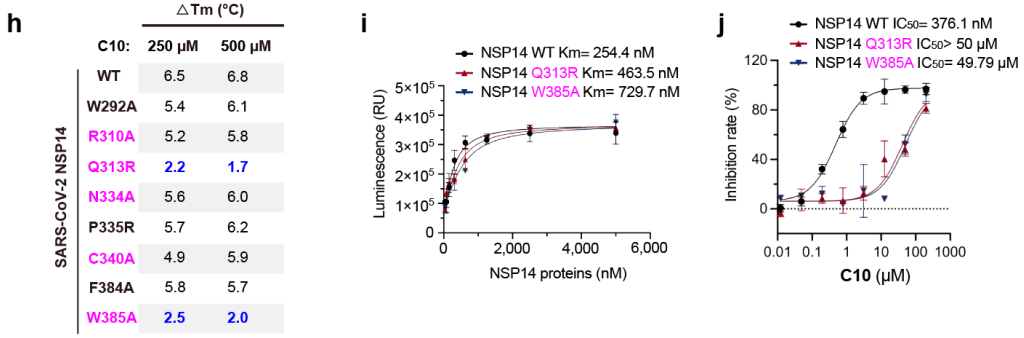

Fig. 3h. Summary of the ΔTm values for 250 μM and 500 μM C10 binding with SARS-CoV-2 NSP14 wild-type and mutants. **i**. Titration of NSP14 and mutants at 1.5 μM SAM and 1.5 μM GpppG for Km value determination. n = 3. Data are shown as mean ± SD. **j**. Dose-dependent inhibition curves of C10 against SARS-CoV-2 NSP14 wild-type, Q313R and W385A as measured by the MTase-Glo assay.

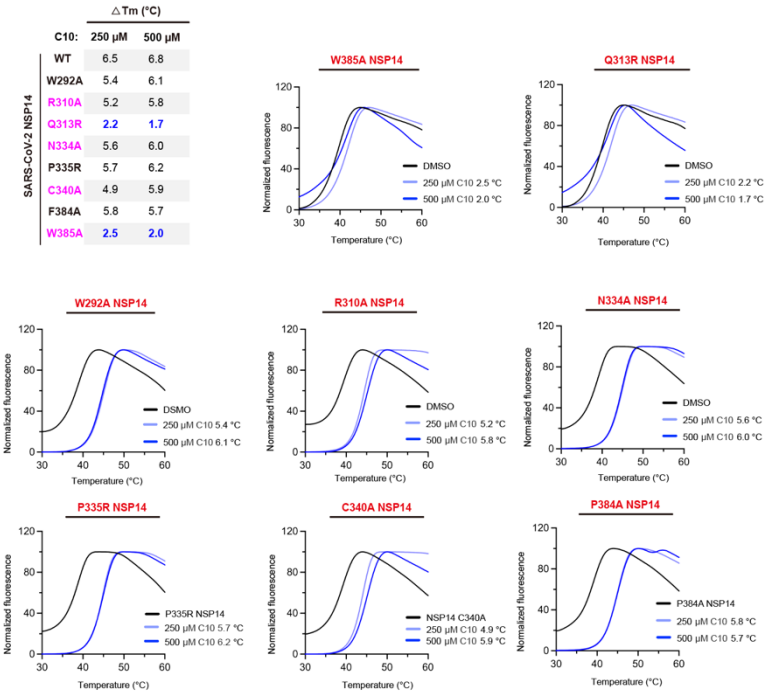

Extended Data Fig. 8. Melting temperature shifts of SARS-CoV-2 NSP14 mutants by adding 250 μM and 500 μM C10, as measured by the DSF assays.

We have incorporated these new data into the revised manuscript as follows:

198 To validate the key C10-binding sites on NSP14, we generated a series of single-point mutants
199 (W292R, R310A, Q313R, N334A, P335R, C340A, F384A, and W385A) and assessed their interactions
200 with C10 in DSF assays. Wild-type NSP14 exhibited a ΔTm of 6.5 °C and 6.8 °C with 250 and 500 μM
201 C10 treatment (**Fig. 3h**). In contrast, all mutants displayed reduced ΔTm values when incubating with C10,
202 of which Q313R and W385A mutants, located in the defined site-C, showed the most significantly reduced
203 ΔTm values of 2.2 and 2.5 °C, respectively (**Fig. 3h**, **Extended Data Fig. 8**), indicating the critical role of
204 these residues in C10 binding. We next evaluated the effects of Q313R and W385A mutations in the
205 N7-MTase enzymatic assays. Interestingly, both Q313R and W385A mutants retained N7-MTase activity
206 comparable to that of wild-type (WT) NSP14 (**Fig. 3i**). However, both the Q313R mutation (IC_{50} > 50 μM)
207 and the W385A mutation (IC_{50} = 49.79 μM) caused a drastic loss of C10's inhibitory activity compared
208 with wild-type NSP14 (IC_{50} = 376.1 nM) (**Fig. 3j**) These results indicate that Q313 and W385 are critical
209 residues for C10 binding without affecting the intrinsic catalytic activity of NSP14.

6.Selectivity Studies

To strengthen the manuscript, the authors should report C10's activity against MERS-CoV nsp14, given the zoonotic risk associated with this virus. Additionally, testing C10 against the human N7-MTase involved in mRNA capping is crucial to assess potential off-target effects, especially in light of the compound's in vivo toxicity at high doses (300 mg/kg in mice).

Response:

We thank the reviewer for raising this important point regarding the selectivity profile of C10. To address these concerns, we performed comprehensive selectivity studies assessing C10's activity against both the human RNA guanine-7 methyltransferase (RNMT) and MERS-CoV NSP14.

To evaluate potential off-target effects on the host methyltransferase, we developed a fluorescence polarization (FP) assay for human RNMT using a SAM-FITC probe under optimized assay conditions (20 mM Tris-HCl pH 8.0, 50 mM NaCl, 1 mM DTT, 0.05% Tween-20). The apparent binding affinity (Km) of hRNMT for the SAM-FITC probe was determined to be 862.6 nM (**Extended Data Fig. 2f**). In the assays containing 1 μM hRNMT and 40 nM SAM-FITC, the positive control sinefungin yielded an IC_{50} of 9.02 μM, consistent with its known broad-spectrum methyltransferase inhibition. In contrast, C10 showed no detectable inhibition of hRNMT even at concentrations up to 200 μM (**Fig. 1i**)

To explore the cross-reactivity of C10 against other coronaviruses, we next assessed its activity against MERS-CoV NSP14 using the MTase-Glo assay under standardized conditions (1.5 μM SAM and 1.5 μM GpppG). The Km value for MERS-CoV NSP14 under these conditions was determined to be 573.4 nM (**Extended Data Fig. 2e**). In inhibition assays with 600 nM enzyme,

C10 demonstrated potent activity with an IC_{50} of 671.7 nM, outperforming sinefungin (IC50 = 1.55 μM) under identical conditions (**Fig. 1e**).

Together, these findings show that C10 exhibits strong cross-reactivity against MERS-CoV NSP14, highlighting its broad-spectrum anti-coronaviral potential. Importantly, its lack of inhibition against human RNMT suggests that the observed in vivo toxicity at high doses (300 mg/kg in mice) is unlikely to be mediated through host N7-methyltransferase inhibition. These results support the selective targeting of the conserved viral NSP14 N7-MTase by C10 and strengthen its profile as a promising antiviral lead compound.

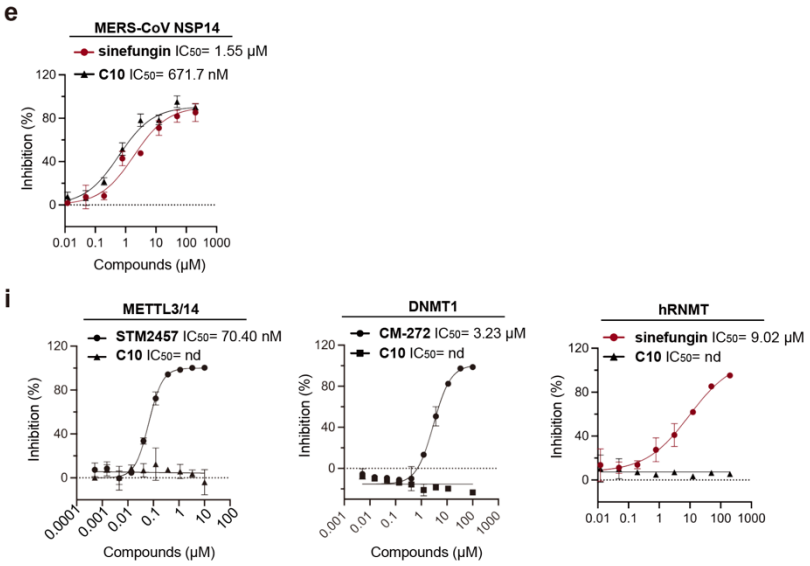

Fig. 1e. Dose-response inhibition curves of C10 and reference compound sinefungin against MERS-CoV NSP14, as measured by the MTase-Glo assay. Data are mean ± SD from three independent replicates. **i**. Selectivity profile of C10 against human methyltransferases: METTL3/14 (compared with STM2457), DNMT1 (compared with CM-272), and RNMT (compared with sinefungin). Data are mean ± SD from three independent replicates.

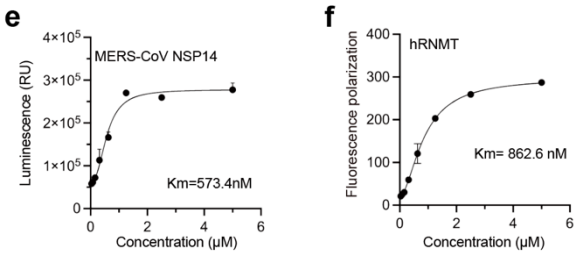

Extended Data Fig. 2e. Titration of MERS-CoV NSP14 at 1.5 μM SAM and 1.5 μM GpppG for Km value determination. n = 3. Data are shown as mean ± SD. **f.** Titration of hRNMT for Km value determination as measured by the FP assay. n = 3. Data are shown as mean ± SD.

We have incorporated the data of MERS-CoV NSP14 into the revised manuscript as follows:

C10 is a selective inhibitor of betacoronavirus NSP14

To evaluate whether C10 exhibits the broad-spectrum inhibitory activity against betacoronavirus NSP14, we assessed its inhibition of MERS-CoV NSP14 (**Extended Data Fig. 2e**), given the zoonotic risk it shares with SARS-CoV-2[46]. It revealed approximately two-fold lower potency compared to SARS-CoV-2 NSP14, exhibiting an IC_{50} value of 671.7 nM (**Fig. 1e**). We also prepared the NSP14 of HCoV-OC43,

We have incorporated the data of hRNMT into the revised manuscript as follows:

To further test the target selectivity of C10, we tested the inhibitory effects of C10 against human methyltransferases, including m6A writer METTL3/14[49], DNA m5C methyltransferase DNMT1[50], and human mRNA cap guanine-N7 methyltransferase (hRNMT, **Extended Data Fig.2f**)[51]. In biochemical assays, C10 showed no detectable inhibitory activity against any of these enzymes (**Fig. 1i**). We also examined whether C-family compounds interfere with the ExoN activity of NSP14. Using an exonuclease assay with the purified NSP14-10 complex[52], neither C3 nor C10 inhibited ExoN activity (**Fig. 1j , Extended Data Fig. 2g**). These results demonstrate that C-family compounds selectively inhibit the N7-MTase activity of NSP14 without affecting its ExoN function, thereby supporting their mechanism as highly specific methyltransferase inhibitors.

Minor Comments

1. Introduction – Functional Coupling of ExoN and MTase Domains

Please mention that although nsp14 has two distinct domains (ExoN and N7-MTase), mutagenesis studies suggest functional interdependence between them. This is important for understanding the enzyme's biology.

Response:

We appreciate the reviewer's insightful suggestion regarding the functional interplay between the ExoN and N7-MTase domains of NSP14. In response, we have expanded the introduction to incorporate structural and mutagenesis evidence demonstrating their interdependence. These additions emphasize NSP14's bifunctional mechanism and its implications for viral pathogenesis and antiviral targeting.

The revised introduction is shown as follows:

Coronaviruses employ their own RNA capping machinery to synthesize the 5′-end cap of viral RNAs in the cytoplasm[6], mimicking host mRNA to promote viral replication and evade innate immune sensing[7–10]. SARS-CoV-2 nonstructural protein 14 (NSP14) is a bifunctional enzyme composed of two distinct domains: a 3′–5′ exoribonuclease (ExoN) domain for viral RNA proofreading[11,12] and an N7-guanosine methyltransferase (N7-MTase) domain that catalyzes the methylation of the guanine-N7 position of viral RNA[13]. Notably, mutagenesis and structural studies suggest a strong functional interdependence between these two domains, by forming a tightly coupled structural framework that supports coordinated regulation of viral RNA proofreading and capping[14–16]. Loss-of-function mutations in either domain have been shown to severely impair viral viability[17–19], highlighting the essential role of NSP14 in viral replication and its potential as a therapeutic target[11,20–22]. In addition, the individual

2. Introduction – SAM-Binding Site as a Drug Target

The sentence "However, the development of promising inhibitors targeting the NSP14 SAM-binding pocket remains underexplored" is somewhat misleading. Several groups have reported inhibitors of this pocket, including adenosine mimetics and bisubstrate analogs. While their efficacy in infected cells is limited, they demonstrate potent in vitro inhibition of N7-MTase activity. Please cite these studies for context.

Response:

We thank the reviewer for this valuable comment. We agree that several groups have indeed reported inhibitors targeting the SAM-binding site of NSP14, including adenosine mimetics and bisubstrate analogs. We have now cited these key studies in the revised "Introduction" to provide appropriate context and acknowledge the prior efforts in this area.

As noted in those reports, however, most SAM-competitive inhibitors are limited by poor cellular permeability and a lack of demonstrated antiviral efficacy in infected cell models or in *vivo*. In this context, C10 represents a notable advancement, which not only selectively inhibits NSP14 N7-MTase activity in vitro but also exhibits broad-spectrum anti-betacoronavirus activity and efficacy in a SARS-CoV-2-infected mouse model. We have revised the manuscript to clarify this distinction and emphasize the translational potential of C10.

The catalytic pocket of NSP14 N7-MTase includes the S-adenosylmethionine (SAM, the universal methyl donor)-binding site and the N7-guanosine RNA cap-binding site. The structural features of NSP14 within its SAM-binding pocket are distinct from those of human methyltransferases, make it an ideal target for highly selective drug design[14,24–29]. Several nucleotide-based inhibitors of NSP14's SAM-binding pocket have been reported, including adenosine mimetics and bisubstrate analogs[30–38]. While these compounds demonstrate potent *in vitro* inhibition of N7-MTase activity, their efficacy in infected cells remains limited. In contrast, the reported non-nucleotide NSP14 inhibitors have generally exhibited lower biopotency and limited target selectivity[39–43]. Until very recently, a first-in-class small molecule inhibitor targeting the NSP14 RNA cap-binding site was disclosed, demonstrating promising antiviral activity and significant therapeutic potential[44]. However, highly potent non-nucleotide inhibitors specifically targeting the SAM-binding pocket of NSP14 with *in vivo* efficacy have not yet been reported. Moreover, the pharmacological effects of NSP14 inhibitors on host-virus interactions and their underlying mechanisms are still poorly understood.

3. Selectivity Studies

It would be beneficial to assess C10's activity against MERS-CoV nsp14 and human N7-MTase to evaluate cross-reactivity and to unravel the toxicity described in mouse model.

Response:

We sincerely appreciate the reviewer's valuable suggestion about the selectivity of C10. Our evaluation demonstrates that C10 exhibits potent inhibition against MERS-CoV NSP14 with an IC_{50} of 671.7 nM in the MTase-Glo assay, compared to 1.55 μM for sinefungin as positive control, confirming its broad-spectrum inhibition against NSP14 of betacoronaviruses including SARS-CoV-2, MERS-CoV and OC43. Importantly, fluorescence polarization assay revealed exceptional selectivity, C10 showed negligible activity against human RNMT (IC_{50} >200 μM) compared to sinefungin (IC_{50} = 9.02 μM). This remarkable selectivity likely comes from evolutionary conservation of the SAM-binding pocket of NSP14 among beta-coronavirus, while it also maintains minimal inhibition against human RNMT.

Please refer to our response to the major comment 6 for additional details.

4. Results – Terminology Clarification

Please clarify the terms "standard precision" and "extra precision" modes in the context of docking analysis. Also, define MPXV at its first mention.

Response:

We thank the reviewer for this helpful suggestion to clarify the terminology used in our docking analysis.

In the revised manuscript, we have now clearly defined the terms **Standard Precision (SP)** and **Extra Precision (XP)** as they apply to molecular docking. SP and XP refer to two distinct docking protocols implemented in the Schrödinger Glide suite, which differ in computational complexity and accuracy. SP mode is optimized for high-throughput virtual screening and employs simplified scoring functions with limited conformational sampling, treating the receptor as rigid and focusing on speed over precision. In contrast, XP mode is designed for more refined docking applications, such as lead optimization. It incorporates more extensive ligand sampling, penalizes non-physical interactions, and includes enhanced scoring functions that account for hydrophobic enclosure and solvent effects. XP docking provides higher accuracy in pose prediction and binding free energy estimation, though it is significantly more computationally intensive (typically 10–50× slower than SP). To assist readers in understanding the computational context of our study, we have now included this clarification in the relevant section.

Additionally, we have defined **MPXV (monkeypox virus)** at its first mention in the manuscript to avoid ambiguity. We appreciate the reviewer's attention to detail, which has helped improve the clarity and accessibility of the text.

The description about SP and XP has been added to the *Materials and Methods* section as follows:

662 atomic number of more than 100. The SP mode employs basic molecular mechanics force fields and
663 simplified scoring functions, incorporating limited ligand conformational sampling while maintaining
664 receptor rigidity, making it suitable for rapid filtration in large-scale virtual screening. A maximum of ten

668 next screening, which adopted the extra precision (XP) algorithm. The XP mode integrates hybrid QM/MM
669 methods with refined scoring functions, enabling extensive conformational sampling including receptor
670 key residue flexibility through rotamer library sampling, along with explicit solvation models to provide
671 more accurate binding mode predictions during lead optimization stages. The parameter settings of the

5. Materials and Methods – Biosafety Level

The biosafety level (BSL) used for experiments involving infectious SARS-CoV-2 should be explicitly stated.

Response:

In response, we have explicitly clarified the biosafety levels used in our viral experiments in the *Materials and Methods* section of the revised manuscript. All experiments involving live SARS-CoV-2 were performed in Biosafety Level 3 (BSL-3) containment facilities in accordance with institutional and national biosafety guidelines. Experiments involving the SARS-CoV-2 transcription and replication-competent virus-like particle (trVLP) system were conducted under Biosafety Level 2 (BSL-2) conditions with enhanced precautions, as recommended for pseudo-typed viral systems.

1104 All experiments involving SARS-CoV-2 trVLP virus infection were performed in the biosafety level 2
1105 (BSL-2) facility of Fudan University. All experiments involving SARS-CoV-2 virus infection were performed
1106 in the biosafety level 3 (BSL-3) facility of Fudan University following the approved SOPs. SARS-CoV-2
1107 replicon assay was performed in the biosafety level 2 (BSL-2) facility of Fudan University.

6 Figure 3e/f – Structural Insights

The authors should discuss their findings in light of previously reported SAM entry gate in nsp14 structures (PMID 36546776).

Response:

We thank the reviewer for the insightful suggestion to contextualize our structural findings in light of the previously described SAM entry gate in NSP14 (PMID: 36546776). In response, we have carefully reviewed this study and expanded our structural interpretation accordingly.

Previous crystallographic analyses (PMID 36546776) have identified a highly dynamic extended loop (residues 356–378) as the SAM entry gate of NSP14. In our predicted structure, this loop adopts an "open" conformation, allowing accommodation of C10, and thus could block SAM access or disrupt its binding, supporting a potential mechanism of competitive inhibition at the SAM-binding site (**Fig. 3d**). In contrast, the "closed" conformation of the loop, as observed in other structures, would not be compatible with C10 binding due to significant steric overlap with the core structure of C10 (**Extended Data Fig. 7f**).

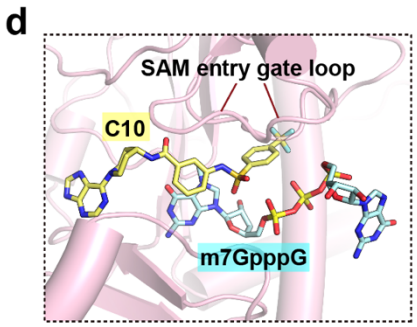

Fig. 3d. An expanded view of C10 and m7GpppG bound to the NSP14 catalytic pocket. C10 and m7GpppG are shown in pale yellow and cyan, respectively, in stick representations. NSP14 is shown in pink, cartoon (top) and surface (bottom) representation.

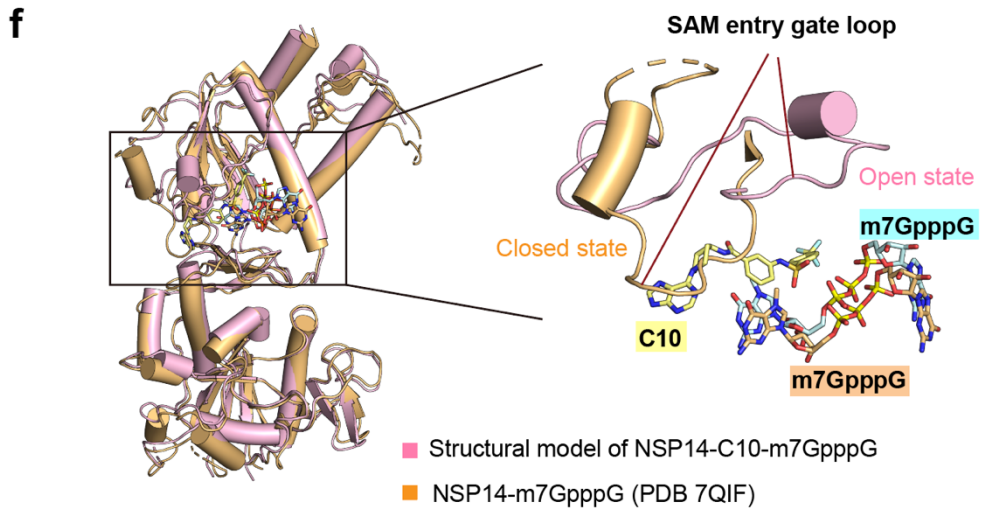

Extended Data Fig. 7f. Structural alignment of the molecular docking model of NSP14-C10-m7GpppG with the crystal structure of NSP14-m7GpppG (PDB ID: 7QIF). An expanded view highlights the dynamic nature of the SAM entry gate loop, which, in its closed conformation, significantly overlaps with the core structure of C10.

The revised text is shown as follows:

trifluoromethyl group (R1 part) of C10 extends out from the binding pocket of SAH (**Fig. 3f**). It was previously reported that an highly dynamic extended loop (residues 356–378) acts as the SAM entry gate of NSP14[27]. This SAM entry gate is in "open" state to embrace C10 in our predicted structure (**Fig. 3d**), while the closed conformation of this loop would not appear to be compatible with binding of C10 as it significantly overlaps with the core structure of C10 (**Extended Data Fig. 7f**). The enhanced potency of

7. Line 164 – Language Editing

The term "authentic" could be removed for clarity, unless it refers to a specific assay

or strain type.

Response:

We thank the reviewer for pointing this out. As suggested, we have removed words of "authentic" in the revised manuscript to increase clarity.

8. Cell Cycle Arrest Section

The section discussing nsp14-induced cell cycle arrest is underdeveloped mechanistically and lacks appropriate controls (e.g., catalytically inactive mutants). As it does not significantly contribute to the main conclusions, it should either be removed or moved to the supplementary information.

Response:

We sincerely thank the reviewer for the insightful comments regarding the section on NSP14-induced cell cycle arrest. We agree that this section lacks appropriate controls, such as the use of catalytically inactive NSP14 mutants, additional cell lines beyond HEK293T, and in vivo validation, which would be required to draw conclusions about NSP14's role in cell cycle regulation.

While our preliminary findings are consistent with previous reports suggesting a role for NSP14 in SARS-CoV-2 induced cell cycle arrest (Zaffagni et al., *eLife*, 2022; Sui et al., *Signal Transduction and Targeted Therapy*, 2023), we agree that this section does not directly support the central conclusions of our study. In line with the reviewer's recommendation, we have moved the cell cycle arrest data to the Supplementary Information (**Extended Data Fig. 15**).

REVIEWERS' COMMENTS

Reviewer #1 (Remarks to the Author):

I did not have any substantial issues during the first round, and I continue to think that this paper merits publication in nature communications. It presented a non-nucleoside inhibitor of the SARS-CoV-2 NSP14 SAM-binding pocket, C10, which demonstrates robust antiviral activity against SARS-CoV-2. In response to other reviewers' comments, the authors have further improved the manuscript.

Response:

We sincerely thank the reviewer for their continued support and positive evaluation of our work. We are especially grateful for the reviewer's recognition of our efforts to improve the manuscript in response to other reviewers' comments.

Reviewer #2 (Remarks to the Author):

I am satisfied by the response to my comments, the authors performed experiments that strengthen the conclusions of the study.

Response:

We sincerely thank the reviewer for their positive feedback and are grateful that the additional experiments and revisions have addressed the concerns and helped to strengthen the conclusions of the study.

Reviewer #3 (Remarks to the Author):

In its revised version, the article by Mengxin Luo et al., "SARS-CoV-2 NSP14 inhibitor exhibits potent antiviral activity and reverses NSP14-driven host modulation", addresses the vast majority of the reviewers' comments. The additional information provided is important and strongly supports the conclusions of the study, which represents a preliminary step toward the development of antivirals targeting the SARS-CoV-2 N7-methyltransferase. I therefore recommend the publication of the revised manuscript in Nature Communications.

Response:

We sincerely thank the reviewer for the thoughtful and encouraging comments. We are grateful that the additional data and revisions were found to adequately address the reviewers' concerns. Thank you for recommending the revised manuscript for publication.

However, a few sentences remain incomplete or difficult to understand. I therefore recommend a careful proofreading of the manuscript prior to publication. Specific points that require correction include:

Lines 201–211: delete the expression "in the experimental end".

Response: As suggested, we have deleted this expression.

Lines 310–311: the sentence "c10 did not disrupt the RNA capping but limits cap N7 methylation" is ambiguous and should be reformulated more clearly.

Response:

We appreciate the reviewer's insightful comment. In the original sentence (Lines 310–311):

"These findings suggest that C10, by inhibiting NSP14 MTase activity, disrupts mRNA capping, thereby selectively suppressing viral translation without broadly affecting host protein synthesis."

We agree that this sentence was ambiguous. Specifically, while C10 inhibits the N7-methyltransferase activity of NSP14, it does not interfere with the initial formation of the RNA cap structure (such as guanosine capping), but rather impairs the N7 methylation step, which is critical for proper cap maturation and recognition by the translation machinery. This selective inhibition is consistent with the observed suppression of viral translation, while host protein synthesis remains largely unaffected.

We have revised the sentence in the manuscript to improve clarity and precision: "*These findings suggest that C10, by inhibiting NSP14 MTase activity, impairs cap maturation step of viral mRNA capping, thereby selectively suppressing viral translation without broadly affecting host protein synthesis.*"

Lines 334–335: please clarify the expression "multiple antiviral effect", which is currently difficult to understand.

Response: We thank the reviewer for pointing this out. We have updated this sentence with explanation: "*Our current findings provide preliminary proof-of-concept that NSP14 inhibition exhibits multiple antiviral effects, including suppression of viral translation, induction of immunostimulatory effects, and reversal of host transcriptome modulation.*"